



**DynaS+
R&D department**



**Dilip Bhalsod in a Toyota Landcruiser
safely takes picture of elephant**



BETA CAE Systems S.A.



ESI's new European HPC center





FEA Information Inc.

A publishing company founded April 2000 – published monthly since October 2000.

The publication's focus is engineering technical solutions/information.

FEA Information Inc. publishes:

FEA Information Engineering Solutions

FEA Information Engineering Journal

FEA Information China Engineering Solutions

Livermore Software Technology, Corp. (LSTC) Developer of LS-DYNA One Code Methodology.

LS-DYNA provides fully integrated, strongly coupled, solvers for extensive multiphysics capabilities. Integrated, at no additional cost. Optimized for shared and distributed memory for Unix, Linux, & Windows Based platforms.

FEA Information Engineering Solutions – Dedicated To:

Finite Element Analysis * Hardware * Software * Cloud * Consulting * CAD * CAE
Distribution* * Implicit * Explicit *Applications * Press Releases * Events * Training



FEA Information
Platinum Participants

logo courtesy - Lancemore





FEA Information News Sections

- 02 FEA Information Inc. Profile
- 03 Platinum Participants
- 05 TOC
- 06 Announcements

Articles – Blogs - News

- 07 DynaS+ launches its R&D department with two aerospace projects
- 09 ESI's new European HPC center Benefits from the Latest Datacenter Infrastructures by Legrand
- 12 BETA CAE Systems S.A. announces the release of the maintenance version 16.0.2 of its software suite.
- 16 Dilip Bhalsod's Great Adventure - Tanzania
- 17 Conference 13th Annual UK Oasys LS-DYNA Users' Meeting
- 18 FEA Information Inc. 2016 LS-DYNA Conference Reception
- 20 14th International LS-DYNA Users Conference
- 22 FAQ LSTC

Automotive & Aerospace Will Return January 2016

LS-DYNA Resources

- Participant Training Courses
- Participant Solutions
- Distribution/Consulting
- Cloud/On Demand/ Subscription
- Models - THUMS - ADT - Barrier
- Social Media

Publication Showcase

LS-DYNA® Smoothed Particle Galerkin (SPG) Method

Yong Guo C.T. Wu and Wei Hu - Livermore Software Technology Corporation

LS-DYNA® Peridynamics for Brittle Fracture Analysis

Bo Ren, C. T Wu - Livermore Software Technology Corporation
E. Askari - Technical Fellow, Boeing Commercial Airplane

Best Fit and Its Application in Metal Forming

Xinhai Zhu, Li Zhang, Yuzhong Xiao - Livermore Software Technology Corporation,

Oasys LS-DYNA UK Users' Meeting 2016 - Thursday 28th January 2016**14th International LS-DYNA Conference**

Abstracts have been accepted and notices have been sent.

For sponsorships contact vic@lstc.com

Courtesy Announcement from Tony DeVarco, SGI

tdevarco@sgi.com

White paper is Available: Characterizing LS-DYNA® Performance on SGI® Systems Using SGI MPInside MPI Profiling Tool. www.sgi.com/pdfs/4553.pdf

Courtesy Announcement from Gregory Szuladzinsk

ggg@bigpond.net.au - www.simulate-events.com

Technical Note No.105 - Aircraft fuselage axially impacting a thick RC slab

www.youtube.com/user/g98765432 - then click Video Manager to see all clips.

title - BOEING 767-200 IMPACTING...

Sincerely,

Marsha Victory Trent Eggleston Marnie Azadian

Suri Bala Dilip Bhalsod Yanhua Zhao

FEA Information Engineering Solutions US Edition

DynaS+ launches its R&D department with two aerospace projects

info@dynasplus.com



DynaS+ is the French, Spanish and Portuguese LS-DYNA distributor providing technical support, trainings, and consulting services to its customers.

Through its multiphysics aspect, the modeling of an air drop sequence is chosen as a scientific demonstrator of new FSI capabilities recently developed within the LS-DYNA software (more specifically using ICFD solver).

In 2014, DynaS+ created a R&D department to promote LS-DYNA in an alternative manner by the intensive use of the new added features in highly innovative R&D projects. More precisely, the aim is to take advantage of innovating methodologies developed within LS-DYNA in R&D collaborative project with different industrial players. As a result, two collaborative projects have been launched in 2015 under the supervision of DynaS+.

The first project, a 3-year project named PARAFU, is funded by the French Ministry of Defense and the French Ministry of Economy. The main goal is to succeed in modeling the complete deployment of a hemispherical parachute from the moment it is

dropped from the plane until it reaches the ground, including the transitional phase when the payload is supported by the parachute sail.

Through its multiphysics aspect, the modeling of an air drop sequence (Picture 1) is chosen as a scientific demonstrator of new FSI capabilities recently developed within the LS-DYNA software (more specifically using ICFD solver). The technologies related to this solver (remeshing, coupling capabilities...) will help to remove some existing numerical locks associated with current modeling. This project is developed in partnership with ICAM Nantes (French laboratory specialized in material characterization) and developers of ICFD solver at LSTC.

DynaS+ launches its R&D department with two aerospace projects

The second project, TANKYOU, is a 2-year project funded by European Union and Midi-Pyrenees Region in France.

The project aims to develop an innovative solution that will ultimately simplify the qualification of cryogenic tanks of rocket launcher. To achieve this goal, the definition and specification of a metamaterial with dynamic and vibratory properties equivalent to those of liquid hydrogen is proposed through an

innovative process coupling an analytical approach, a material by design approach (experimental) and an innovative numerical approach based on the Discrete Element Method (DEM and DEM-BOND) of LS-DYNA. This project is developed in partnership with ISAE-SUPAERO (French engineering school) and ATECA (French SME).

For more information: info@dynasplus.com

Vincent LAPOUJADE

Tel: +33 5 61 44 54 98 / Fax: +33 5 61 44 74 88 / Mobile: +33 6 84 15 11 65

E-mail : v.lapoujade@dynasplus.com

5, avenue Didier Daurat - 31 400 TOULOUSE

www.dynasplus.com



ESI's new European HPC center Benefits from the Latest Datacenter Infrastructures by Legrand

ESI's Point of Delivery for Cloud Computing, based in Teratec Campus

The Great Technical Achievement Behind this new Point of Distribution

Paris, France – December 21, 2015 – ESI Group, pioneer and world-leading solution provider in Virtual Prototyping for manufacturing industries, announces the opening of its new European HPC Center. The datacenter is now based on the Teratec Campus, an ideal location to launch collaborative High-Performance Computing (HPC) projects as it is in the vicinity of Europe's biggest HPC center: the CEA's "Très Grand Centre de Calcul". The new datacenter will effectively act as ESI's POD (Point of Delivery), serving all ESI offices across Europe as a platform for ESI's new software development and engineering services alike. ESI teamed up with Legrand, the global

specialist in electrical and digital building infrastructures to meet the technical challenges surrounding this project.

Based in Teratec Campus For years, Legrand has been supplying integrated solutions for lighting, energy, networks, and access management in buildings. Present in more than 80 countries with a workforce of over 36,000, the Group's mission is to design, develop, and market electrical and digital systems that are both simple and innovative. Since 2009, Legrand has intensified its activity in the UPS (Uninterruptible Power Supply) sector, as required for efficiently operating datacenters aimed at supporting HPC activities, especially with the acquisition of S2S in France.

To build its new datacenter at Teratec, ESI worked with Legrand Datacenter Solutions, a branch specialized in delivering adequate answers to the numerous challenges inherent to supercomputing: from energy efficiency to cooling, security, and scalability. ESI also teamed up with Minkels, a company belonging to the Legrand Group and specializing in datacenter hardware, including housing, UPS, cooling, monitoring and power distribution solutions, together with their partner Cap Ingelec, strong of 20 years' experience in data centers.

"In most buildings, the economic and/or safety and security issues necessitate reliable availability of energy and data and the costs associated with a loss of operation can be very substantial", comments Pascal Perrin, Datacenter Business Development Manager at Legrand. "Our solutions ensure the electrical and digital supply of the data center at all times."

Continuous availability of power supply is of uttermost importance to make sure ESI can run large HPC calculations smoothly, as required to deliver projects at the right time to ESI's industrial customers.

Vincent Chaillou, COO, ESI Group, explains: "ESI successfully completed the implantation of its new datacenter, in collaboration with Legrand. Aside of guaranteeing Uninterrupted Power Supply to support our software and services operations, this intelligent infrastructure is set to adapt to ESI's evolving needs and computational loads. It delivers a scalable, adaptable infrastructure, ready to anticipate the next big technological challenges, including Big Data evolutions and the Internet of Things."

Pascal Perrin adds: "In the era of virtualization and cloud computing, a massive increase in the volume of data is expected: the annual growth in data is expected to rise from 50% in 2010 to reach 4400% in 2020 (1). This rapid growth will have a major impact on how we design our server rooms, with scalability becoming vital."

Other devices installed by Legrand include air filters, protecting equipment from dust that tends to overheat hardware, so these can last longer. The datacenter also benefits from Legrand's energy saving technologies, reducing the ecological footprint of ESI's activities, as part of the company's commitment to the environment and future generations.

Marc Daoud, Account Manager at Minkels, explains: "ESI's new datacenter features Minkel's Cold Corridor®. This technology segregates the cold and hot airflows using advanced air conditioning systems. The housing solution uses specific foam joints to make sure it's airtight. Cold air is pulsed into the external alleys to cool down the supercomputers, and comes out hot into the central alley. The level of cold air absorption obtained is optimum, so that temperature variations are kept to a minimum: temperature inside the rack must remain between 22°C and 28°C. All in all, our technology delivers the best possible environment to run effective operations while protecting hardware and ensure its durability."

Vincent Chaillou concludes: "ESI is now equipped with a Cloud Computing PoD to run state of the art calculations, as required to leverage our developments and engineering studies in the field of Virtual Prototyping. This new PoD actively contributes to achievement of ESI's vision: by granting our customers access to HPC and Cloud Computing, and by democratizing the use of such technologies, we propose a new model to our industrial customers — empowering them to deliver disruptive innovations." (1) Source: Gartner Research

ESI Group – Media Relations

Céline Gallerne +33 1 41 73 58 46

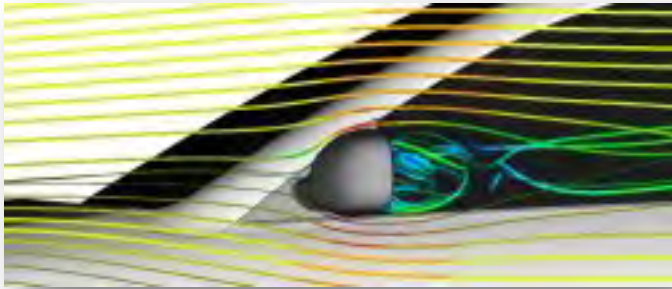
Celine.Gallerne@esi-group.com

About ESI: ESI is a world-leading provider of Virtual Prototyping software and services with a strong foundation in the physics of materials and Virtual Manufacturing

Founded over 40 years ago, ESI has developed a unique proficiency in helping industrial manufacturers replace physical prototypes by virtually replicating the fabrication, assembly and testing of products in different environments. Virtual Prototyping enables ESI's clients to evaluate the performance of their product and the consequences of its manufacturing history, under normal or accidental conditions. By benefiting from this information early in the process, enterprises know whether a product can be built, and whether it will meet its performance and certification objectives, before any physical prototype is built. To enable customer innovation, ESI's solutions integrate the latest technologies in high performance computing and immersive Virtual Reality, allowing companies to bring products to life before they even exist.

Today, ESI's customer base spans nearly every industry sector. The company employs about 1000 high-level specialists worldwide to address the needs of customers in more than 40 countries.

BETA CAE Systems S.A. - release of maintenance version 16.0.2 of its software suite.



This maintenance release is focused on the correction of identified problems and issues for the ANSA and μ ETA software of the BETA CAE Systems suite v16.0x branch, for those who have not migrated to the v16.1x branch yet.

About this release

The 16x version of the ANSA pre-processor provides full compatibility with previous major versions. As with every major release, a broad range of new features and enhancements to existing ones add value to our solutions, reinforce overall process consistency, accelerate user performance, and provide a considerable boost on productivity.

The ϵ tilysis solver is the new addition to the BETA CAE Systems analysis tools family and is available with the ANSA / ϵ tilysis / μ ETA suite. Named after the Greek word for solution, it operates as a solution in the field of Finite Element Analysis embodying the accumulated knowledge from 25 years of collaboration with the CAE community. ϵ tilysis covers numerous solution types and intends to bridge the gap between pre- and post-processing for disciplines such as Structural, NVH, Optimization, and more.

The v16x version of the μ ETA post-processor builds upon the tools available in previous releases, now supporting an increased array of new interfaces including ϵ tilysis, the in-house solver of BETA CAE Systems, as well as enhancing the multi-disciplinary tools.

The most important additions and fixes implemented in v16.0.2 are listed below.

Understanding the Software Release Schedule

The plan

We are committed in delivering improved and enhanced software releases, the soonest possible, in order to meet the requirement of our customers for the continuous improvement of their experience and work. Therefore, we are working in releasing new software versions with code corrections, new software features and enhancements, in regular, frequent intervals.

- A major software version is released every year.
- First point releases, such as v16.0.0, v16.1.0, v16.2.0 and so on, with code corrections but also with additional software features and enhancements are released every three months.
- Second point releases, such as v16.0.1, v16.0.2 etc. mainly with code corrections only upon their parent first point release, are scheduled on a monthly basis.

Each software release is accompanied by a detailed description of the introduced corrections and/or additions so that our customers can decide whether it is critical to implement this release in their environment.

This release: This release of v16.0.2 brings additional features and code corrections on v16.0.x.

Known issues resolved in ANSA

General

Launch: The default starting .sh script in Linux machines has been modified to search both for lockfile and socket instead of only lockfile.

Clicking twice inside the 'List of Coordinate Systems to Compress' window, could result in unexpected termination.

In some cases, Laminates would be illustrated with an improper offset position.

Scripting

ExtractCrossSectionsFromPlane(): Running the function in nogui mode, resulted in unexpected termination.

Output: The “use_relative_name_for_readonly_includes” option of an output script function (eg., OutputNastran()), would not be applied.

CAD Import / Export: CATIA Working planes in CATIA files would be converted to Faces during import in ANSA.

Connections and Assembly:

In certain cases the realization of Seam Lines Y-JOINT-SHELL would fail if affected elements belonged to Morphing Boxes.

Meshing

Save As: Attempting to save a copy from a compressed database (.ansa.gz) would result in a non-compressed file.

Elements Wrap [Variable Length]: The “Scale Base Length” option might not be respected by the procedure.

Refine: Trias function would not apply on Linked Faces.

Solver Interfaces

OptiStruct : New parameters are now supported through OptiStruct output function.

LS-DYNA: The Spot Welds Checks procedure might ignore Contact of Type TIED_SHELL_EDGE_TO_SURFACE_OFFSET.

Simulayt: Layup files output by ANSA , could not be read in by Primer due to a missing field on the 202 lines.

For more details about the new software features, enhancements and corrections please, refer to the Release Notes document.

Compatibility and Supported Platforms

ANSA files saved by all the first and second point releases of a major version are compatible to each other. New major versions can read files saved by previous ones but not vice versa.

μETA Project files saved from version 16.0.2 are compatible and can be opened by μETA version 16.0.0 or later. To be readable by μETA versions earlier than v16.0.0, they have to be saved selecting the option "Version <16.0.0".

Support for 32-bit platform has been discontinued for all operating systems.

Where to download from

Customers who are served directly by BETA CAE Systems, or its subsidiaries, may download the new software, examples and documentation from their account on our server. They can access their account through the "user login" link at our web site.

Contact us if you miss your account details. The [PublicDir] link will give you access to the public downloads area.

Customers who are served by a local business agent should contact the local support channel channel for software distribution details.

What to download

All files required for the installation of this version reside in the folder named "BETA_CAE_Systems_v16.0.2" and are dated as of December 18, 2015. These files should replace any pre-releases or other files downloaded prior to that date.

The distribution of this version of our pre- and post-processing suite is packaged in one, single, unified installation file, that invokes the

respective installer and guides the procedure for the installation of the required components.

For the installation of the software on each platform type, the.sh installer file residing in the folder with respective platform name, for Linux and MacOS or the respective .msi installer file for Windows, 64bit, have to be downloaded.

In addition to the above, optionally, the μ ETA Viewer is available to be downloaded for each supported platform.

The tutorials and the example files reside in the folder named "TUTORIALS". This folder includes the complete package of the tutorials and example files, and a package with only the updated ones.

The Abaqus libraries required for the post-processing of Abaqus .odb files are included in the installation package and can be optionally unpacked.

Earlier software releases are also available in the sub-directory called "old" or in a folder named after the product and version number.

www.facebook.com/betacae

www.beta-cae.com/mobile_app.htm

www.youtube.com/user/betacae

www.linkedin.com/company/beta-cae-systems-s-a-

<https://plus.google.com/104877716929629946383/posts>

<http://twitter.com/betacae>

Dilip Bhalsod's Great Adventure - Tanzania



Conference 13th Annual UK Oasys LS-DYNA Users' Meeting

Website: http://www.oasys-software.com/dyna/en/events/users_jan-16/users_jan-16.shtml

13th Annual UK Oasys LS-DYNA Users' Meeting

Location: Arup Campus, Solihull, UK

The thirteenth in a series of update meetings for Oasys LS-DYNA Users will be held at the Arup office in Solihull, UK, on Thursday 28th January 2016.

As in previous years this event will bring together around 100 UK users of the Oasys and LS-DYNA software to provide information on upcoming features of Oasys and LS-DYNA, and to learn more about current and new applications, as well as other related software products.

We are looking forward to talks from the Oasys team at Arup as well as special guest speakers, Brian Wainscott and Paul Du Bois

The event will be followed by a complimentary meal at The Boot Inn in Lapworth. Please note that The Boot Inn has a limited capacity so please ensure you register in advance to ensure your place at the evening meal.

Registration This event is free of charge. To register for the event and the evening meal simply send an email with your company/affiliation and contact details to [Alison Harper](mailto:alison.harper@oasys-software.com). Please also let us know if you have any particular dietary requirements when you register.

Please note: in line with our company sustainability policy we do not plan to provide printed copies of the presentations for each attendee at the event; the presentations will be made available to download after the event. If you particularly require a printed copy on the day please let us know when you register.



14TH International LS-DYNA Users Conference - Welcome Reception Sunday, June 12, 2016

FEA Information Inc., D3View and the following FEA Information Participating LS-DYNA distributors will be hosting the Welcome Reception at the 14th International LS-DYNA Conference .

During the reception each participant will be announced giving you the opportunity to meet and know the FEA Information LS-DYNA's global representatives. We will be adding additional co-sponsors to our list each month.
Please join us in 2016

From China:

- Shanghai Hengstar Technology Co., Ltd.
- Dalian Fukun
- ARUP China

From Korea:

- THEME
- KOrea Simulation TEChnology Co.,Ltd

From Sweden:

- DYNAmore Nordic AB

From Germany:

- DynaMORE GmbH
- CADFEM GmbH

From India:

- Kaizenat Technologies Pvt. Ltd.
- Arup India Pvt Ltd

From the US

- Dynamax
- LSTC

From the UK

- ARUP UK

From France

- DynaS+

Keynote speaker Paul DuBois who will be presenting a joint presentation at the conference:

A new versatile tool for simulation of failure in LS-DYNA and the application to aluminum extrusions

- **Paul Du Bois, Consulting engineer**
- **Dr. Tobias Erhart, Dr. Filipe Andrade, Dr. Andre Haufe, Dynamore GmbH**
- **Drs. Frieder Neukamm, Dr. Markus Feucht, Daimler AG**

Presentation Contents

- **Aluminium extrusions**
- **Material modeling of Aluminium extrusions**
- **Concept of a generalized failure model**
- **Example of anisotropic damage**
- **Example of volumetric/deviatoric damage**
- **Plane stress anisotropic failure : directional dependency upon the state of stress**
- **Failure model for aluminum extrusion**
- **Example of a bumper component**
- **Conclusions**



Welcome The conference will host a forum for engineers, professors, students, consultants, industry leaders, and interested parties to exchange their ideas, and listen to the latest in industry and academic presentations..

The presenter (1) of the accepted paper will receive a complimentary (no fee) registration, when they register using the “LSTC Conference Registration,” at the Royal Dearborn Hotel.

Corporate Participation: Platinum, Gold, Silver, Bronze

Conference Dates

Sunday, June 12, 2016:

Registration Exhibition Area, Reception

Monday, June 13, 2016:

Registration Exhibition Area Banquet

Tuesday, June 14, 2016:

Registration Exhibition Area Closing

Wednesday & Thursday, June 15 & 16, 2016:

Training Classes

Contact Information

Abstracts & papers:

papers@lstc.com

Participation, Registration:

Marsha Victory vic@lstc.com

Abstract Submission

- Deadline: November 30, 2015
- Length: Approx. 300 words, include figures
- Format: 7” x 8½”, MS Word template provided

Notification: December 31, 2015

Paper Submission

- Deadline: March 05, 2016
- Length: 3,000 word maximum
- Format: 8½” x 11” paper, single-spaced
MS Word template provided

Conference Schedule & Training

Sunday, June 12, 2016:

- Registration for early arrivals,
- Training opportunities during day
- Exhibitors open in evening,
- Reception

Monday, June 13:

- Registration,
- Conference,
- Banquet

Tuesday, June 14, 2016.

- Registration,
- Conference
- Closing session - about 3pm

Wednesday, June 15

Thursday, June 16

- 1& 2-day Training at U-M Dearborn

Conference Sponsorship and Booth Information

For information on Sponsorships and Booths please contact Marsha vic@lstc.com

Previous Sponsors and Exhibitors: If you would like the same booth that you hosted, at the last conference, please let me know so I can quickly reserve your booth placement.



AUTOMOTIVE NEWS & EVENTS

WILL RETURN IN JANUARY 2016



AEROSPACE NEWS & EVENTS

WILL RETURN IN JANUARY 2016



LS-DYNA Multiphysics YouTube Facundo Del Pin

WILL RETURN IN JANUARY 2016

FAQs

LSTC provide a huge number of FAQs at the ftp site [ftp.lstc.com/outgoing/support/FAQ](ftp://ftp.lstc.com/outgoing/support/FAQ). Many thanks to Jim Day of LSTC for making this information available.

Some specific popular FAQs include:

consistent units

ftp://ftp.lstc.com/outgoing/support/FAQ/consistent_units

An overview of Contact

<ftp://ftp.lstc.com/outgoing/support/FAQ/contact.overview>

Soft Contact

<ftp://ftp.lstc.com/outgoing/support/FAQ/contact.soft1>

General guidelines for Crash Analysis

<ftp://ftp.lstc.com/outgoing/support/FAQ/guidelines.pdf>

Hourglass Control

ftp://ftp.lstc.com/outgoing/support/FAQ/hourglass_condensed

Dealing with Instabilities

<ftp://ftp.lstc.com/outgoing/support/FAQ/instability.tips>

Dealing with long run times

ftp://ftp.lstc.com/outgoing/support/FAQ/long_run_times

Mass Scaling

ftp://ftp.lstc.com/outgoing/support/FAQ/mass_scaling

Negative Volume in Brick Elements

ftp://ftp.lstc.com/outgoing/support/FAQ/negative_volume_in_brick_element.tips

Quasi-static simulations

<ftp://ftp.lstc.com/outgoing/support/FAQ/quasistatic>

Restarting Analyses

<ftp://ftp.lstc.com/outgoing/support/FAQ/restart>

Modeling spinning bodies

<ftp://ftp.lstc.com/outgoing/support/FAQ/spin>

Spring Back

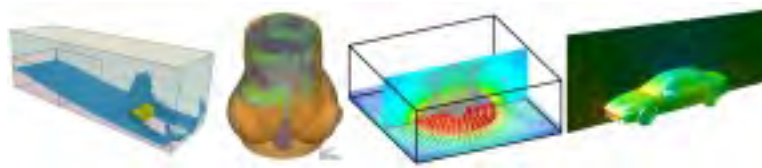
<ftp://ftp.lstc.com/outgoing/support/FAQ/springback>

Stress vs Strain for plasticity models

ftp://ftp.lstc.com/outgoing/support/FAQ/stress_vs_strain_for_plasticity_models

User-defined materials

ftp://ftp.lstc.com/outgoing/support/FAQ/user_defined_materials.faqFAQs



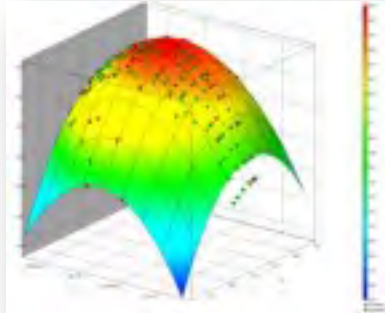
LS-DYNA Support

At this site you will find answers to basic and advanced questions that might occur while using LS-DYNA, information about new releases and ongoing developments.

2015 Recent Changes

The Support Website has the direct pdfs for the following October Updates

- History Variables for Certain Material Models
- LS-DYNA Manual R 8.0 - Vol III
- LS-DYNA Manual R 8.0 - Vol II
- LS-DYNA Manual R 8.0 - Vol I



LS-OPT

LS-OPT, the graphical optimization tool that interfaces perfectly with LS-DYNA,

Allows the user to structure the design process, explore the design space and compute optimal designs according to specified constraints and objectives. The program is also highly suited to the solution of system identification problems and stochastic analysis.

The graphical tool LS-OPTui interfaces with LS-DYNA and provides an environment to specify optimization input, monitor and control parallel simulations and post-process

optimization data, as well as viewing multiple designs using LS-PREPOST.

Optimization

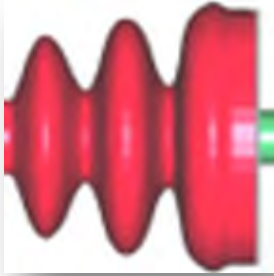
- Size-/Shape optimization
- Constraints, mixed continuous/discrete variables, multiple load cases, etc.
- Multi-Objective optimization (Pareto Frontier)
- Reliability based design optimization

LS-TaSC - LS-TaSC 3.1 released

Topology Optimization

A tool for the topology optimization of non-linear problems involving dynamic loads and contact conditions. It can be used to find a

concept design for most structures analyzed using LS-DYNA.



LS-DYNA Examples

The site presents approximately 200 LS-DYNA examples from various training classes. The input files and several class notes are available for download.

The download is free of charge, a login is not required. The majority of content has been contributed by LSTC/DYNAmore. The content is prepared for educational purposes. Hence, material properties and other parameters might be non-physic for simplification.

Among the files and Sections:

LS-DYNA Keyword Search If you are looking for an example containing some specific LS-DYNA keyword you may use the site search in the header section of this page.

Show Cases This folder contains several LS-DYNA examples focusing on specific load cases or keywords.

Metal Forming The examples in this section are from the introductory class on metal forming from LSTC. You may access the examples separately by the menu on the left. The examples are prepared for LS-DYNA 970 and upwards.

ALE The examples in this section are from the ALE (Arbitrary Lagrangian Eulerian Method) class of M'hamed Souli. M'hamed Souli is

Professor at the University in Lille France. Both authors are key developers for the powerful capabilities of the Eulerian Methods in LS-DYNA. You may access the examples separately by using the menu on the left. The examples run with LS-DYNA 970 and upwards.

Thermal The examples in this section present examples about the thermal capabilities of LS-DYNA. The examples are provided by Dr. Art Shapiro. Art is working since decades on topics related to DYNA3D, LS-DYNA and TOPAZ. He is the key developer for the thermal capabilities of LS-DYNA. Art is one of the co-founders of LSTC. You may access the examples separately by using the menu on the left.



DYNAlook

DYNAlook

The site presents papers from European and International LS-DYNA User Conferences and papers provided by other users. 1604 papers are available.

The papers are from LS-DYNA Conferences and are accessible via the search functionality.

2015 will be published soon.

**13th International
LS-DYNA Conference**
Detroit, 2014

**9th European
LS-DYNA Conference**
Manchester, 2013

**12th International
LS-DYNA Conference**
Detroit, 2012

**8th European LS-DYNA
Conference**
Straßburg, 2011 ...

DUMMY Model Support - Currently, the manuals of models developed by DYNAmore are available.

This site provides detailed information on dummy models for LS-DYNA. In the near future the models developed by LSTC will be added. The LSTC dummy and barrier are models are no fee and included with the LS-DYNA license.

To license the models we kindly ask to contact your local LS-DYNA distributor. Any kind of proposal or enhancements for the models and this site is very welcome.

Among the Dummy Models on this site you can find:

Side Impact Dummies

ES2/ES2re -
DYNAmore

World SID 50%
DYNAmore

US-SID
DYNAmore

Rear Impact Dummies

BioRID-II V3.
DYNAmore

Child Dummies

P-1.5
DYNAmore
P-3.0
DYNAmore

LSTC Models Overview

Free or low cost FE models are important to LS-DYNA users in various fields. Therefore, LSTC is developing models with the help and support of our customers. Some of the models are joint developments with our partners.

LSTC's Models are available at no cost to licensees of LS-DYNA who are current with their annual license fees (Annual License) or maintenance fees (Paid-up License). Models are fully unencrypted and accessible. LSTC endeavors to make the models as complete, accurate, reliable, and easy to use as possible.

This section of our site was created to keep users informed about our models. It will be

Barrier Models

LSTC offers several Offset Deformable Barrier (ODB) and Movable Deformable Barrier (MDB) models:

- ODB modeled with shell elements
- ODB modeled with solid elements
- ODB modeled with a combination of shell and solid elements
- MDB according to FMVSS 214 modeled with shell elements
- MDB according to FMVSS 214 modeled with solid elements
- MDB according to ECE R-95 modeled with shell elements
- AE-MDB modeled with shell elements
- IIHS MDB modeled with shell elements
- IIHS MDB modeled with solid elements
- RCAR bumper barrier
- RMDB modeled with shell and solid elements

updated periodically to reflect changes to existing models and announce newly released models.

Feedback about the models is welcome and will be used to improve future releases. To submit questions, suggestions, or feedback about LSTC's models, please send an e-mail to: atds@lstc.com.

For news and updates about our dummy models, please join our models news mailing list.

www.lstc.com/products/models/maillinglist

AEROSPACE WORKING GROUP

<http://awg.lstc.com/tiki/tiki-index.php>

The **LS-DYNA® Aerospace Working Group (AWG)** is a partnership of federal agencies, corporations, and universities working together to develop and publish aerospace test cases and modeling guidelines for finite element analyses with LS-DYNA®.

The actions of the AWG serve to support the use, development, and reliability of LS-DYNA® for aerospace numerical analyses.

Some participants are partially or fully funded by the Federal Aviation Administration (FAA) in the National Aviation Research Plan 'Aircraft Catastrophic Failure Prevention Research' program, or by the National Aeronautics and Space Administration (NASA), or associated with the participants as LS-DYNA® users.

Engine Related Impact Failure (ERIF) - Arizona State University (ASU)

- Boeing
- Central Connecticut State University (CCSU)
- Federal Aviation Administration (FAA)
- General Electric Aviation
- George Mason University (GMU)
- Honda Aircraft Engine
- Honeywell
- Livermore Software Technology Corporation (LSTC)
- National Aeronautics and Space Administration (NASA)

- Ohio State University (OSU)
- Pratt & Whitney
- Pratt & Whitney Canada
- Rolls-Royce
- University of Akron
- Williams International

Cabin Interior (CI)

- B/E Aerospace
- Boeing
- Bombardier
- Central Connecticut State University
- Cessna
- Federal Aviation Administration (FAA)
- Humanetics
- National Aeronautics and Space Administration (NASA)
- Wichita State University
- Zodiac Aerospace



Participant's Training Classes

Webinars

Info Days

Class Directory

Participant Class Directory

Arup (corporate)	www.oasys-software.com/dyna/en/training
BETA CAE Systems S.A. (corporate)	www.beta-cae.com/training.htm
DYNAMore (corporate)	www.dynamore.de/en/training/seminars
ESI-Group (corporate)	https://myesi.esi-group.com/trainings/schedules
ETA (corporate)	www.eta.com/support2/training-calendar
LSTC (corporate)	www.lstc.com/training
LS-DYNA OnLine (Al Tabiei)	www.LSDYNA-ONLINE.COM

ARUP Visit the website for complete listings/changes/locations

www.oasys-software.com/dyna/en/training

To enrol on any of these courses please email Dyna Support at dyna.support@arup.com.

Date	Training Class
26-27 January 2016	Polymeric Material Modelling in LS-DYNA
Scheduled on request	Oasys PRIMER - An Introduction
Scheduled on request	Oasys PRIMER - Automatic Assembly of Multiple Crash Cases
Scheduled on request	Oasys PRIMER - Spotwelds and Connections
Scheduled on request	Oasys PRIMER - Seat and Dummy Positioning
Scheduled on request	Oasys PRIMER & D3PLOT - An Introduction to JavaScripting

BETA CAE Visit the website for complete listings/changes/locations

www.beta-cae.com/training.htm

Basic and advanced training courses can be scheduled upon request. A variety of standard or tailored training schedules, per product or per discipline, are being offered to meet customers needs.

A number of recommended training courses offered are described below. The list is not exhaustive and more courses can be designed according to your needs.

Please, contact ansa@beta-cae.gr for further details.

Recommended Training Courses (Complete information on website)

- SPDRM
- ANSA / μ ETA Basics
- ANSA / μ ETA for CFD
- ANSA / μ ETA for Crash & Safety simulation
- ANSA / μ ETA for Durability simulation
- ANSA / μ ETA for NVH analyses
- Multi-Body Dynamics
- Laminated Composites
- Morphing and Optimization
- Automation
- Additional special sessions

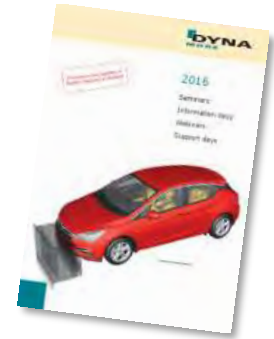
DYNAmore Visit the website for complete listings / changes / locations

www.dynamore.de/seminars

New seminar brochure for 2016 published by DYNAmore

Download (pdf): www.dynamore.de/seminars-2016

We are pleased to offer you our new seminar brochure for 2016. Once again, we have adapted our extensive range of seminars and free-of-charge information events to current developments as well as the needs of our customers.



With the newly founded DYNAmore subsidiary DYNAmore France SAS, selected seminars are now also offered in the new office in Versailles.

Selection of trainings and free-of-charge information & support days in the first quarter of 2016

Forming Simulation with eta/DYNAFORM	28-29 Jan.
Hot Forming with LS-DYNA	26-27 Jan.
Crash Analysis with LS-DYNA	1-4 Feb. (L, only few vacancies left)
Joining Techniques for Crash Analysis	10-11 Feb. (L) / 1-2 March
Introduction to LS-PrePost	15 Feb. / 14 March
Introduction to LS-DYNA	16-18 Feb. / 15-17 March
Parameter Identification with LS-OPT	19 Feb. / 8 March (L)
User Interfaces in LS-DYNA	29 Feb.
Implicit Analysis with LS-DYNA	3-4 March
Introduction to Passive Safety Simulation	10-11 March
Damage and Failure Modeling	15-16 March (T) / 15-16 March (G)
CPM for Airbag Modeling	18 March
ALE and Fluid-Structure Interaction	21-22 March (V)
Information day: Possibilities with LS-DYNA/Implicit	23 Feb.
Information day: ANSA, LS-OPT and META	29 Feb.
Information day: Welding and Heat Treatment	7 March
Information day: PRIMER (Preprocessor for LS-DYNA)	8 March
Support day: LS-DYNA	15 Jan. / 19 Feb.
Support day: Occupant Safety	18 March

If not otherwise stated, the event location is Stuttgart, Germany. Other event locations are:
 L = Linköping, Sweden; G = Göteborg, Sweden; T = Turin, Italy; V = Versailles, France

Overview and registration: www.dynamore.de/seminars

If the offered seminars do not fully suit your needs, we are pleased to meet your individual requirements by arranging tailored on-site training courses on your company premises.

DYNAmore hopes that our offer will meet your needs and would be very pleased to welcome you at one of the events.

<https://myesi.esi-group.com/trainings/schedules>

6 Jan 2016 to 7 Jan 2016

Basic OpenFOAM training for application engineers

20 Jan 2016 to 22 Jan 2016

PAM-STAMP for the automotive industry (Group Learning)

LSTC Visit the website for complete listings/changes/locations

www.lstc.com/training

January Training

- **MI Intro LS-PrePost**
- **MI Intro LS-DYNA**
- **MI Blast In LS-DYNA**

February Training

- **CA ALE/Eulerian/FSI**
- **CA SPH**

March

- **MI Intro LS-PrePost**
- **MI Intro LS-DYNA**

May

- **CA Intro LS-PrePost**
- **CA Intro LS-DYNA**
- **MI Contact**
- **MI Composite**

LS-DYNA Visit the website for complete listings/changes/locations
On Line www.LSDYNA-ONLINE.COM

For Information contact: courses@lsdyna-online.com or 513-3319139

Composite Materials In LS-DYNA

This course will allow first time LS-DYNA users to use composite materials. The most important elements to start using all the composite material models in LS-DYNA will be presented in the 8 hours.

Foam & Viscoelastic Materials in LS-DYNA

Objective of the course: Learn about several foam material models in LS-DYNA to solve engineering problems. Detailed descriptions are given of the data required to use such material in analysis. Examples are used to illustrate the points made in the lectures

Plasticity, Plastics, and Viscoplastic Materials in LS-DYNA

Objective of the course: Learn about several plasticity based material models in LS-DYNA to solve engineering problems. Detailed descriptions are given of the data required to use such material in analysis. Examples are used to illustrate the points made in the lectures.

Rubber Materials in LS-DYNA

Objective of the course: Learn about several rubber material models in LS-DYNA to solve engineering problems. Detailed descriptions are given of the data required to use such material in analysis. Examples are used to illustrate the points made in the lectures.



BETA CAE Systems S.A.

www.beta-cae.gr

BETA CAE Systems S.A.– ANSA

An advanced multidisciplinary CAE pre-processing tool that provides all the necessary functionality for full-model build up, from CAD data to ready-to-run solver input file, in a single integrated environment. ANSA is a full product modeler for LS-DYNA, with integrated Data Management and Process Automation. ANSA can also be directly coupled with LS-OPT or LSTC to provide an integrated solution in the field of optimization.

Solutions for:

Process Automation - Data Management – Meshing – Durability - Crash & Safety NVH - CFD - Thermal analysis - Optimization - Powertrain Products made of composite materials - Analysis Tools - Maritime and Offshore Design - Aerospace engineering - Biomechanics

BETA CAE Systems S.A.– μETA

Is a multi-purpose post-processor meeting diverging needs from various CAE disciplines. It owes its success to its impressive performance, innovative features and capabilities of interaction between animations, plots, videos, reports and other objects. It offers extensive support and handling of LS-DYNA 2D and 3D results, including those compressed with SCAI's FEMZIP software



CRAY

www.cray.com

THE CRAY® XC™ SERIES: ADAPTIVE SUPERCOMPUTING ARCHITECTURE

The Cray® XC™ series delivers on Cray's commitment to an adaptive supercomputing architecture that provides both extreme scalability and sustained performance. The flexibility of the Cray XC platform ensures that users can precisely configure the machines that will meet their specific requirements today, and remain confident they can upgrade and enhance their systems to address the demands of the future.

Cray® XC40™ and XC40-AC™ supercomputers are enabled by a robust Intel® Xeon® processor road map, Aries high performance interconnect and flexible Dragonfly network topology, providing low latency and scalable global bandwidth to satisfy the most challenging multi-petaflops applications.

While the extreme-scaling Cray XC40 supercomputer is a transverse air-flow liquid-cooled architecture, the Cray XC40-AC air-cooled model provides slightly smaller and less dense supercomputing cabinets with no requirement for liquid coolants or extra blower cabinets. A reduced network topology lowers costs, and the system is compatible with the compute technology, OS, ISV and software stack support of high-end XC40 systems.

MAXIMIZE PRODUCTIVITY WITH CRAY CS SERIES SUPERCOMPUTERS

Understanding the need for nimble, reliable and cost-effective high performance computing (HPC), we developed the Cray® CS™ cluster supercomputer series. These systems are industry-standards-based, highly customizable, and expressly designed to handle the broadest range of medium- to large-scale simulation and data analytics workloads.

All CS components have been carefully selected, optimized and integrated to create a powerful HPC environment. Flexible node configurations featuring the latest processor and interconnect technologies mean you can tailor a system to your specific need — from an all-purpose cluster to one suited for shared memory, large memory or accelerator-based tasks.

Innovations in packaging, power, cooling and density translate to superior energy efficiency and compelling price/performance. Expertly engineered system management software instantly boosts your productivity by simplifying system administration and maintenance.

Maximize your productivity with flexible, high-performing Cray CS series cluster supercomputers.

CRAY

www.cray.com**CRAY® SONEXION® SCALE-OUT LUSTRE® STORAGE SYSTEM**

Brought to you by Cray, the world's leading experts in parallel storage solutions for HPC and technical enterprise, the Cray® Sonexion® 2000 system provides a Lustre®-ready solution for popular x86 Linux® clusters and supercomputers through Cray Cluster Connect™. As a leader in open systems and parallel file systems, Cray builds on open source Lustre to unlock any industry-standard x86 Linux compute cluster using InfiniBand™ or 10/40 GbE utilizing proven Cray storage architectures.

The Cray Sonexion 2000 system provides 50 percent more performance and capacity than the Sonexion 1600 system in the same footprint.

Simplify

- Through its fully-integrated and pre-configured design, Cray Sonexion storage gets customers deployed faster and reduces the total number of components to manage.
- The Sonexion system's compact design reduces the total hardware footprint of petascale systems by 50 percent over component-based solutions.

Scale

- Performance scales from 7.5 GB/s to 1.7 TB/s in a single file system.
- Capacity scales in modular increments; the Sonexion 2000 system stores over two usable petabytes in a single rack. Fewer drives and components reduce capital costs as capacity grows.

Protect

- New software-based GridRAID offers higher levels of data protection and up to 3.5 times faster rebuild times than traditional RAID6 and MD-RAID storage.
- Cray ensures quality, reliability and stability at scale through exhaustive thermal and real-world stress testing, system hardening and availability, and tight hardware and software integration.

OPEN ARCHIVE AND TIERED STORAGE SYSTEM FOR BIG DATA AND SUPERCOMPUTING

Cray Tiered Adaptive Storage (TAS), powered by Varsity, is designed to meet the expansive data preservation and access needs driven by big data, where data needs to migrate fluidly from high performance storage to deep tape archives, while always being accessible to users.

CRAY

www.cray.com**With Cray TAS you can:**

- Deploy tiered storage and archives faster
- Feel confident preserving and protecting data into the future, using Linux®
- Simplify managing data using familiar tools for years to come

CRAY® URIKA-XA™ EXTREME ANALYTICS PLATFORM

Pre-integrated, open platform for high performance analytics delivers valuable business insights now and into the future

The flexible, multi-use Cray® Urika-XA™ extreme analytics platform addresses perhaps the most critical obstacle in data analytics today — limitation. Analytics problems are getting more varied and complex but the available solution technologies have significant constraints. Traditional analytics appliances lock you into a single approach and building a custom solution in-house is so difficult and time consuming that the business value derived from analytics fails to materialize.

In contrast, the Urika-XA platform is open, high performing and cost effective, serving a

wide range of analytics tools with varying computing demands in a single environment. Pre-integrated with the Apache Hadoop® and Apache Spark™ frameworks, the Urika-XA system combines the benefits of a turnkey analytics appliance with a flexible, open platform that you can modify for future analytics workloads. This single-platform consolidation of workloads reduces your analytics footprint and total cost of ownership.

Based on pioneering work combining high-performance analytics and supercomputing technologies, the Urika-XA platform features next-generation capabilities. Optimized for compute-heavy, memory-centric analytics, it incorporates innovative use of memory-storage hierarchies and fast interconnects, which translates to excellent performance at scale on current as well as emerging analytics applications.

Additionally, the enterprise-ready Urika-XA platform eases the system management burden with a single point of support, standards-based software stack and compliance with enterprise standards so you can focus on extracting valuable business insights, not on managing your environment.

CRAY

www.cray.com

THE URIKA-GD™ GRAPH DISCOVERY APPLIANCE IS A PURPOSE-BUILT SOLUTION FOR BIG DATA RELATIONSHIP ANALYTICS.

The Urika-GD™ appliance enables enterprises to:

- Discover unknown and hidden relationships and patterns in big data
- Build a relationship warehouse, supporting inferencing/deduction, pattern-based queries and intuitive visualization
- Perform real-time analytics on the largest and most complex graph problems

The Urika-GD system is a high performance graph appliance with a large shared memory and massively multithreaded custom processor designed for graph processing and scalable I/O.

With its industry-standard, open-source software stack enabling reuse of existing skill sets and no lock in, the Urika-GD appliance is easy to adopt.

The Urika-GD appliance complements an existing data warehouse or Hadoop® cluster by offloading graph workloads and interoperating within the existing enterprise analytics workflow.

Realize rapid time to powerful new insights.



DatapointLabs

www.datapointlabs.com

Testing over 1000 materials per year for a wide range of physical properties, DatapointLabs is a center of excellence providing global support to industries engaged in new product development and R&D.

The company meets the material property needs of CAE/FEA analysts, with a specialized product line, TestPaks®, which allow CAE analysts to easily order material testing for the calibration of over 100 different material models.

DatapointLabs maintains a world-class testing facility with expertise in physical properties of plastics, rubber, food, ceramics, and metals.

Core competencies include mechanical, thermal and flow properties of materials with a focus on precision properties for use in product development and R&D.

Engineering Design Data including material model calibrations for CAE Research Support Services, your personal expert testing laboratory Lab Facilities gives you a glimpse of our extensive test facilities Test Catalog gets you instant quotes for over 200 physical properties.



ETA – Engineering Technology Associates

etainfo@eta.com

www.eta.com

Inventium Suite™

Inventium Suite™ is an enterprise-level CAE software solution, enabling concept to product. Inventium's first set of tools will be released soon, in the form of an advanced Pre & Post processor, called PreSys.

Inventium's unified and streamlined product architecture will provide users access to all of the suite's software tools. By design, its products will offer a high performance modeling and post-processing system, while providing a robust path for the integration of new tools and third party applications.

PreSys

Inventium's core FE modeling toolset. It is the successor to ETA's VPG/PrePost and FEMB products. PreSys offers an easy to use interface, with drop-down menus and toolbars,

increased graphics speed and detailed graphics capabilities. These types of capabilities are combined with powerful, robust and accurate modeling functions.

VPG

Advanced systems analysis package. VPG delivers a unique set of tools which allow engineers to create and visualize, through its modules--structure, safety, drop test, and blast analyses.

DYNAFORM

Complete Die System Simulation Solution. The most accurate die analysis solution available today. Its formability simulation creates a "virtual tryout", predicting forming problems such as cracking, wrinkling, thinning and spring-back before any physical tooling is produced



ESI Group

www.esi-group.com

Visual-Environment is an integrative simulation platform for simulation tools operating either concurrently or standalone for various solver. Comprehensive and integrated solutions for meshing, pre/post processing, process automation and simulation data management are available within same environment enabling seamless execution and automation of tedious workflows. This very open and versatile environment simplifies the work of CAE engineers across the enterprise by facilitating collaboration and data sharing leading to increase of productivity.

Visual-Crash DYNA provides advanced preprocessing functionality for LS-DYNA users, e.g. fast iteration and rapid model revision processes, from data input to visualization for crashworthiness simulation and design. It ensures quick model browsing, advanced mesh editing capabilities and rapid graphical assembly of system models. Visual-Crash DYNA allows graphical creation, modification and deletion of LS-DYNA entities. It comprises tools for checking model quality and simulation parameters prior to launching calculations with the solver. These

tools help in correcting errors and fine-tuning the model and simulation before submitting it to the solver, thus saving time and resources.

Several high productivity tools such as advanced dummy positioning, seat morphing, belt fitting and airbag folder are provided in **Visual-Safe**, a dedicated application to safety utilities.

Visual-Mesh is a complete meshing tool supporting CAD import, 1D/2D/3D meshing and editing for linear and quadratic meshes. It supports all meshing capabilities, like shell and solid automesh, batch meshing, topo mesh, layer mesh, etc. A convenient Meshing Process guides you to mesh the given CAD component or full vehicle automatically.

Visual-Viewer built on a multi-page/multi-plot environment, enables data grouping into pages and plots. The application allows creation of any number of pages with up to 16 windows on a single page. These windows can be plot, animation, video, model or drawing block windows. Visual-Viewer performs automated tasks and generates customized reports and thereby increasing engineers' productivity.



ESI Group

www.esi-group.com

Visual-Process provides a whole suite of generic templates based on LS-DYNA solver (et altera). It enables seamless and interactive process automation through customizable LS-DYNA based templates for automated CAE workflows.

All generic process templates are easily accessible within the unique framework of Visual-Environment and can be customized upon request and based on customer's needs.

VisualDSS is a framework for Simulation Data and Process Management which connects with Visual-Environment and supports product

engineering teams, irrespective of their geographic location, to make correct and realistic decisions throughout the virtual prototyping phase. *VisualDSS* supports seamless connection with various CAD/PLM systems to extract the data required for building virtual tests as well as building and chaining several virtual tests upstream and downstream to achieve an integrated process. It enables the capture, storage and reuse of enterprise knowledge and best practices, as well as the automation of repetitive and cumbersome tasks in a virtual prototyping process, the propagation of engineering changes or design changes from one domain to another.

Latest Release is Visual-Environment v11.0

**JSOL Corporation**

www.jsol.co.jp/english/cae/

HYCRASH

Easy-to-use one step solver, for Stamping-Crash Coupled Analysis. HYCRASH only requires the panels' geometry to calculate manufacturing process effect, geometry of die are not necessary. Additionally, as this is target to usage of crash/strength analysis, even forming analysis data is not needed. If only crash/strength analysis data exists and panel ids is defined. HYCRASH extract panels to calculate it's strain, thickness, and map them to the original data.

JSTAMP/NV

As an integrated press forming simulation system for virtual tool shop

the JSTAMP/NV meets the various industrial needs from the areas of automobile, electronics, iron and steel, etc. The JSTAMP/NV gives satisfaction to engineers, reliability to products, and robustness to tool shop via the advanced technology of the JSOL Corporation.

JMAG

JMAG uses the latest techniques to accurately model complex geometries, material properties, and thermal and structural phenomena associated with electromagnetic fields. With its excellent analysis capabilities, JMAG assists your manufacturing process



Livermore Software Technology Corp.

www.lstc.com

LS-DYNA

A general-purpose finite element program capable of simulating complex real world problems. It is used by the automobile, aerospace, construction, military, manufacturing, and bioengineering industries. LS-DYNA is optimized for shared and distributed memory Unix, Linux, and Windows based, platforms, and it is fully QA'd by LSTC. The code's origins lie in highly nonlinear, transient dynamic finite element analysis using explicit time integration.

LS-PrePost: An advanced pre and post-processor that is delivered free with LS-DYNA. The user interface is designed to be both efficient and intuitive. LS-PrePost runs on Windows, Linux, and Macs utilizing OpenGL graphics to achieve fast rendering and XY plotting.

LS-OPT: LS-OPT is a standalone Design Optimization and Probabilistic Analysis package with an interface to LS-DYNA. The graphical preprocessor LS-OPTui facilitates

definition of the design input and the creation of a command file while the postprocessor provides output such as approximation accuracy, optimization convergence, tradeoff curves, anthill plots and the relative importance of design variables.

LS-TaSC: A Topology and Shape Computation tool. Developed for engineering analysts who need to optimize structures, LS-TaSC works with both the implicit and explicit solvers of LS-DYNA. LS-TaSC handles topology optimization of large non-linear problems, involving dynamic loads and contact conditions.

LSTC Dummy Models:

Anthropomorphic Test Devices (ATDs), as known as "crash test dummies", are life-size mannequins equipped with sensors that measure forces, moments, displacements, and accelerations.

LSTC Barrier Models: LSTC offers several Offset Deformable Barrier (ODB) and Movable Deformable Barrier (MDB) model.



Oasys Ltd. LS-DYNA Environment

The Oasys Suite of software is exclusively written for LS-DYNA® and is used worldwide by many of the largest LS-DYNA® customers. The suite comprises of:

Oasys PRIMER

Key benefits:

- Pre-Processor created specifically for LS-DYNA®
- Compatible with the latest version of LS-DYNA®
- Maintains the integrity of data
- Over 6000 checks and warnings – many auto-fixable
- Specialist tools for occupant positioning, seatbelt fitting and seat squashing (including setting up pre-simulations)
- Many features for model modification, such as part replace
- Ability to position and de-penetrate impactors at multiple locations and produce many input decks

www.oasys-software.com/dyna

- automatically (e.g. pedestrian impact, interior head impact)
- Contact penetration checking and fixing
- Connection feature for creation and management of connection entities.
- Support for Volume III keywords and large format/long labels
- Powerful scripting capabilities allowing the user to create custom features and processes

www.oasys-software.com/dyna

Oasys D3PLOT

Key benefits:

- Powerful 3D visualization post-processor created specifically for LS-DYNA®
- Fast, high quality graphics
- Easy, in-depth access to LS-DYNA® results
- Scripting capabilities allowing the user to speed up post-processing, as well as creating user defined data components



Oasys T/HIS

Key benefits:

- Graphical post-processor created specifically for LS-DYNA®
- Automatically reads all LS-DYNA® results
- Wide range of functions and injury criteria
- Easy handling of data from multiple models
- Scripting capabilities for fast post-processing

Oasys REPORTER

Key benefits:

- Automatic report generation tool created specifically for LS-DYNA®
- Automatically post-process and summarize multiple analyses
- Built-in report templates for easy automatic post-processing of many standard impact tests



Shanghai Hengstar

Center of Excellence: Hengstar Technology is the first LS-DYNA training center of excellence in China. As part of its expanding commitment to helping CAE engineers in China, Hengstar Technology will continue to organize high level training courses, seminars, workshops, forums etc., and will also continue to support CAE events such as: China CAE Annual Conference; China Conference of Automotive Safety Technology; International Forum of Automotive Traffic Safety in China; LS-DYNA China users conference etc.

On Site Training: Hengstar Technology also provides customer customized training programs on-site at the company facility. Training is tailored for customer needs using LS-DYNA such as material test and input keyword preparing; CAE process automation with customized script program; Simulation result correlation with the test result; Special topics with new LS-DYNA features etc..

www.hengstar.com

Distribution & Support: Hengstar distributes and supports LS-DYNA, LS-OPT, LS-Prepost, LS-TaSC, LSTC FEA Models; Hongsheng Lu, previously was directly employed by LSTC before opening his distributorship in China for LSTC software. Hongsheng visits LSTC often to keep update on the latest software features.

Hengstar also distributes and supports d3View; Genesis, Visual DOC, ELSDYNA; Visual-Crash Dyna, Visual-Process, Visual-Environment; EnkiBonnet; and DynaX & MadyX etc.

Consulting

As a consulting company, Hengstar focus on LS-DYNA applications such as crash and safety, durability, bird strike, stamping, forging, concrete structures, drop analysis, blast response, penetration etc with using LS-DYNA's advanced methods: FEA, ALE, SPH, EFG, DEM, ICFD, EM, CSEC..

**Lenovo**www.lenovo.com

Lenovo is a USD39 billion personal and enterprise technology company, serving customers in more than 160 countries.

Dedicated to building exceptionally engineered PCs, mobile Internet devices and servers spanning entry through supercomputers, Lenovo has built its business on product innovation, a highly efficient global supply

chain and strong strategic execution. The company develops, manufactures and markets reliable, high-quality, secure and easy-to-use technology products and services.

Lenovo acquired IBM's x86 server business in 2014. With this acquisition, Lenovo added award-winning System x enterprise server portfolio along with HPC and CAE expertise.



www.penguincomputing.com

Penguin Computing provides customized build-to-order server solutions for enterprises and institutions with special hardware requirements. We complement our hardware and software solutions with Penguin Computing on Demand (POD)—a public HPC cloud that provides supercomputing capabilities on-demand on a pay-as-you-go basis.

Penguin is a one-stop shop for HPC and enterprise customers, providing solutions for a wide array of computing needs and user profiles:

- HPC and cloud solutions optimized for industry-specific uses

- High-powered workstations for individual power users

- Highly power-efficient server platforms for enterprise computing

- Private and public cloud solutions, including hybrid options.

Focus

Penguin Computing is strictly focused on delivering Linux-optimized enterprise solutions. We use a thorough, proven hardware qualification and testing process to ensure that our solutions deliver optimal performance and robustness.

Penguin's in-house development team is dedicated to providing a complete highly interoperable software stack that is tuned for Penguin hardware. As a result our solutions are easy-to-use and "just work." Our integrated approach even extends to our hybrid compute solutions, which combine local and cloud computing resources, taking ease-of-use and cost-effectiveness to the next level. Penguin customers can reduce capital expenditures by right-sizing clusters for average resource utilization and easily and quickly offload excess workload into the cloud.

Penguin also offers a full range of services and support that is backed by a seasoned team of Linux, HPC and application experts.

Canada **Metal Forming Analysis Corp MFAC** galb@mfac.com
www.mfac.com

LS-DYNA	LS-OPT	LS-PrePost	LS-TaSC
LSTC Dummy Models	LSTC Barrier Models	eta/VPG	
eta/DYNAFORM	INVENTIUM/PreSys		

United States **DYNAMAX** sales@dynamax-inc.com
www.dynamax-inc.com

LS-DYNA	LS-OPT	LS-PrePost	LS-TaSC
LSTC Dummy Models		LSTC Barrier Models	

United
States**ESI-Group N.A**www.esi-group.com

QuikCAST

SYSWELD

PAM-RTM

PAM-CEM

VA One

CFD-ACE+

ProCAST
Process

Visual-

VisualDSS

Weld Planner

Visual-Environment

IC.IDO

United
States**Engineering Technology Associates – ETA**etainfo@eta.comwww.eta.com

INVENTIUM/PreSy

NISA

VPG

LS-DYNA

LS-OPT

DYNAform

United
States**Gompute**www.gompute.cominfo@gompute.com

LS-DYNA Cloud Service

Additional software

Additional Services

United
States**Comet Solutions**steve.brown@cometsolutions.com

Comet Software

United
States

Livermore Software Technology Corp

sales@lstc.com

LSTC www.lstc.com

LS-DYNA

LS-OPT

LS-PrePost

LS-TaSC

LSTC Dummy Models

LSTC Barrier Models

TOYOTA THUMS

United
States

Predictive Engineering

george.laird@predictiveengineering.com

www.predictiveengineering.com

FEMAP

NX Nastran

LS-DYNA

LS-OPT

LS-PrePost

LS-TaSC

LSTC Dummy Models

LSTC Barrier Models

France**DynaS+**v.lapoujade@dynasplus.comwww.dynasplus.com

Oasys Suite

LS-DYNA

LS-OPT

LS-PrePost

LS-TaSC

DYNAFORM

VPG

MEDINA

LSTC Dummy Models

LSTC Barrier Models

Germany**CADFEM GmbH**lsdyna@cadfem.dewww.cadfem.de

ANSYS

LS-DYNA

optiSLang

ESAComp

AnyBody

ANSYS/LS-DYNA

Germany**DYNAmore GmbH**uli.franz@dynamore.dewww.dynamore.de

PRIMER	LS-DYNA	FTSS	VisualDoc
LS-OPT	LS-PrePost	LS-TaSC	DYNAFORM
Primer	FEMZIP	GENESIS	Oasys Suite
TOYOTA THUMS		LSTC Dummy & Barrier Models	

The Netherlands**Infinite Simulation Systems B.V**j.mathijssen@infinite.nlwww.infinite.nl

ANSYS Products	CivilFem	CFX	Fluent
LS-DYNA	LS-PrePost	LS-OPT	LS-TaSC

Italy	EnginSoft SpA	info@enginsoft.it		
	www.enginsoft.it			
	ANSYS	MAGMA	Flowmaster	FORGE
	CADfix	LS-DYNA	Dynaform	Sculptor
	ESAComp	AnyBody	FTI Software	
	AdvantEdge	Straus7	LMS Virtual.Lab	ModeFRONTIER
<hr/>				
Russia	STRELA	info@dynamorussia.com		
	LS-DYNA	LS-TaSC	LS-OPT	LS-PrePost
	LSTC Dummy Models		LSTC Barrier Models	
<hr/>				
Sweden	DYNAMore Nordic	marcus.redhe@dynamore.se		
	www.dynamore.se			
	ANSA	μETA	LS-DYNA	LS-OPT
	LS-PrePost	LS-TaSC	FastFORM	DYNAform
	FormingSuite		LSTC Dummy Models	
		LSTC Barrier Models		
<hr/>				
Sweden	GOMPUTE	info@gridcore.com		
	www.gridcore.se	www.gompute.com		
	LS-DYNA Cloud Service	Additional software		

Switzerland	DYNAmoreSwiss GmbH	info@dynamore.ch	
		www.dynamore.ch	
	LS-DYNA	LS-OPT	LS-PrePost
	LS-TaSC	LSTC Dummy Models	LSTC Barrier Models

UK	Ove Arup & Partners	dyna.sales@arup.com	
		www.oasys-software.com/dyna	
	LS-DYNA	TOYOTA THUMS	LS-PrePost
	LS-TaSC	PRIMER	T/HIS
	REPORTER	SHELL	HYCRASH
	DIGIMAT	Simpleware	LSTC Dummy Models
		LSTC Barrier Models	

China	ETA – China		lma@eta.com.cn		
	www.eta.com/cn				
	Inventium	VPG	DYNAFORM	NISA	
	LS-DYNA	LS-OPT	LSTC Dummy Models	LS-PrePost	
			LSTC Barrier Models	LS-TaSC	
China	Oasys Ltd. China		Stephen.zhao@arup.com		
	www.oasys-software.com/dyna				
	PRIMER	D3PLOT	HYCRASH	T/HIS REPORTER	SHELL
	LS-DYNA		LS-OPT	LSTC Dummy Models	LS-PrePost
	DIGIMAT		FEMZIP	LSTC Barrier Models	LS-TaSC
China	Shanghai Hengstar Technology		info@hengstar.com		
	www.hengstar.com				
	LS-DYNA	LS-TaSC	LSTC Barrier Models	D3VIEW	
	LS-PrePOST	LS-OPT	LSTC Dummy Models		
	Genesis	VisualDoc		ELSDYNA	
	Visual-Crahs DYNA	Visual-Proeces		DynaX & MadyX	
	Enki Bonnet	Visual Environement			

India	Oasys Ltd. India	lavendra.singh@arup.com		
	www.oasys-software.com/dyna			
	PRIMER	D3PLOT	T/HIS	
			LS-OPT	LSTC Dummy Models
				LS-PrePost
			LS-DYNA	LSTC Barrier Models
				LS-TaSC

India	CADFEM Eng. Svce	info@cadfem.in		
	www.cadfem.in			
	ANSYS	VPS	ESAComp	optiSLang
	LS-DYNA	LS-OPT	LS-PrePost	

India	Kaizenat Technologies Pvt. Ltd	support@kaizenat.com		
	http://kaizenat.com/			
	LS-DYNA	LS-OPT	LSTC Dummy Models	LS-PrePost
	Complete LS-DYNA suite of products		LSTC Barrier Models	LS-TaSC

Distribution/Consulting	Asia Pacific	Distribution/Consulting
-------------------------	--------------	-------------------------

Japan	CTC	LS-dyna@ctc-g.co.jp		
	www.engineering-eye.com			
	LS-DYNA	LS-OPT	LS-PrePost	LS-TaSC
	LSTC Dummy Models	LSTC Barrier Models	CmWAVE	

Japan	JSOL		Oasys Suite	
	www.jsol.co.jp/english/cae		JMAG	
	JSTAMP	HYCRASH	LS-PrePost	LS-TaSC
	LS-DYNA	LS-OPT		
	LSTC Dummy Models	LSTC Barrier Models	TOYOTA THUMS	

Japan	FUJITSU			
	http://jp.fujitsu.com/solutions/hpc/app/lsdyna			
	LS-DYNA	LS-OPT	LS-PrePost	LS-TaSC
	LSTC Dummy Models	LSTC Barrier Models	CLOUD Services	

Japan	LANCEMORE	info@lancemore.jp		
	www.lancemore.jp/index_en.html			
	Consulting			
	LS-DYNA	LS-OPT	LS-PrePost	LS-TaSC
	LSTC Dummy Models	LSTC Barrier Models		

Japan	Terrabyte	English:		
	www.terrabyte.co.jp	www.terrabyte.co.jp/english/index.htm		
	Consulting			
	LS-DYNA	LS-OPT	LS-PrePost	LS-TaSC
	LSTC Dummy Models	LSTC Barrier Models	AnyBody	

Korea	THEME	wschung@kornet.com		
	www.lsdyna.co.kr		Oasys Suite	
	LS-DYNA	LS-OPT	LS-PrePost	LS-TaSC
	LSTC Dummy Models	LSTC Barrier Models	eta/VPG	Planets
	eta/DYNAFORM	FormingSuite	Simblow	TrueGRID
	JSTAMP/NV	Scan IP	Scan FE	Scan CAD
	FEMZIP			

Korea	KOSTECH	young@kostech.co.kr		
	www.kostech.co.kr			
	LS-DYNA	LS-OPT	LS-PrePost	LS-TaSC
	LSTC Dummy Models	LSTC Barrier Models	eta/VPG	FCM
	eta/DYNAFORM	DIGIMAT	Simuform	Simpack
	AxStream	TrueGrid	FEMZIP	

Taiwan**Flotrend**gary@flotrend.twwww.flotrend.com.tw

LS-DYNA

LS-OPT

LS-PrePost

LS-TaSC

LSTC Dummy Models

LSTC Barrier Models

eta/VPG

FCM

Taiwan**APIC**www.apic.com.tw

LS-DYNA

LS-OPT

LS-PrePost

LS-TaSC

LSTC Dummy Models

LSTC Barrier Models

eta/VPG

FCM



POD (Penguin Computing on Demand) offers software including LSTC's LS-DYNA

www.penguincomputing.com/services/hpc-cloud

Penguin HPC clusters are optimized for engineering workloads and offer:

- Instant access to an HPC Cloud Cluster
- High performance InfiniBand bare-metal compute
- Free support from HPC experts
- No charges for network transfers
- Cost-effective, pay-per-use billing model
- Secure environment for private data
- Detailed billing reports for user groups and projects

Self Registration Portal – featuring rich--documentation, wiki, FAQ, pricing and more.

<https://pod.penguincomputing.com/>

POD Software Applications and Libraries (visit site for complete listing)

FEA, CFD and FDTD Modeling

- **LS-DYNA / LS-PrePost** LS-DYNA is an advanced general-purpose multiphysics simulation software package. Its core-competency lie in highly nonlinear transient dynamic finite element analysis (FEA) using explicit time integration. LS-PrePost is an advanced pre and post-processor that is delivered free with LS-DYNA.
- **OpenFoam:** OpenFOAM (Open source Field Operation And Manipulation) is a C++ toolbox for the development of customized numerical solvers, and pre-/post-processing utilities for the solution of continuum mechanics problems, including computational fluid dynamics (CFD).



- **ANSYS HFSS:** ANSYS HFSS software is the industry standard for simulating 3-D full-wave electromagnetic fields. Its gold-standard accuracy, advanced solver and compute technology have made it an essential tool for engineers designing high-frequency and high-speed electronic components.
- **ANSYS Fluent** ANSYS Fluent software contains the broad physical modeling capabilities needed to model flow, turbulence, heat transfer, and reactions for industrial applications.
- **Star-CD and Star-CCM+:** STAR-CCM+ is CD-adapco's newest CFD software product. It uses the well established CFD solver technologies available in STAR-CD, and it employs a new client-server architecture and object oriented user interface to provide a highly integrated and powerful CFD analysis environment to users.
- **Convergent:** CONVERGE is a Computational Fluid Dynamics (CFD) code that completely eliminates the user time needed to generate a mesh through an innovative run-time mesh generation technique.
- **Lumerical:** Simulation tools that implement FDTD algorithms.



**Cloud computing services
for
JSOL Corporation LS-DYNA users in Japan**

**JSOL Corporation is cooperating with chosen
cloud computing services**

JSOL Corporation, a Japanese LS-DYNA distributor for Japanese LS-DYNA customers.

LS-DYNA customers in industries / academia / consultancies are facing to the increase use of LS-DYNA more and more in recent years.

In calculations of optimization, robustness, statistical analysis, larger amount of LS-DYNA license in short term are required.

JSOL Corporation is cooperating with some cloud computing services for JSOL's LS-DYNA users and willing to provide large in short term license.

This service is offered to the customers by the additional price to existence on-premises license, which is relatively inexpensive than purchasing yearly license.

The following services are available

Contact; JSOL Corporation Engineering Technology Division cae-info@sci.jsol.co.jp

(only in Japanese).

HPC OnLine

NEC Solution Innovators, Ltd.

http://jpn.nec.com/manufacture/machinery/hpc_online/

Focus

Foundation for Computational Science

<http://www.j-focus.or.jp>

Platform Computation Cloud

CreDist.Inc.

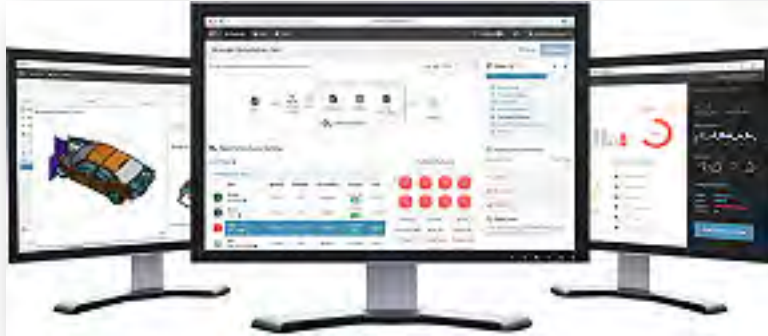
<http://www.credist.co.jp/>

PLEXUS CAE

Information Services International-Dentsu, Ltd.
(ISID) <https://portal.plexusplm.com/plexus-cae/>

SCSK Corporation

<http://www.scsk.jp/product/keyword/keyword07.html>



Rescale: Cloud Simulation Platform

The Power of Simulation Innovation

We believe in the power of innovation. Engineering and science designs and ideas are limitless. So why should your hardware and software be limited? You shouldn't have to choose between expanding your simulations or saving time and budget.

Using the power of cloud technology combined with LS-DYNA allows you to:

- Accelerate complex simulations and fully explore the design space
- Optimize the analysis process with hourly software and hardware resources
- Leverage agile IT resources to provide flexibility and scalability

True On-Demand, Global Infrastructure

Teams are no longer in one location, country, or even continent. However, company data centers are often in one place, and everyone must connect in, regardless of office. For engineers across different regions, this can

cause connection issues, wasted time, and product delays.

Rescale has strategic/technology partnerships with infrastructure and software providers to offer the following:

- Largest global hardware footprint – GPUs, Xeon Phi, InfiniBand
- Customizable configurations to meet every simulation demand
- Worldwide resource access provides industry-leading tools to every team
- Pay-per-use business model means you only pay for the resources you use
- True on-demand resources – no more queues

ScaleX Enterprise: Transform IT, Empower Engineers, Unleash Innovation

The ScaleX Enterprise simulation platform provides scalability and flexibility to companies while offering enterprise IT and management teams the opportunity to expand and empower their organizations.

Rescale Cloud Simulation Platform

ScaleX Enterprise allows enterprise companies to stay at the leading edge of computing technology while maximizing product design and accelerating the time to market by providing:

- Collaboration tools
- Administrative control
- API/Scheduler integration
- On-premise HPC integration

Industry-Leading Security

Rescale has built proprietary, industry-leading security solutions into the platform, meeting the

needs of customers in the most demanding and competitive industries and markets.

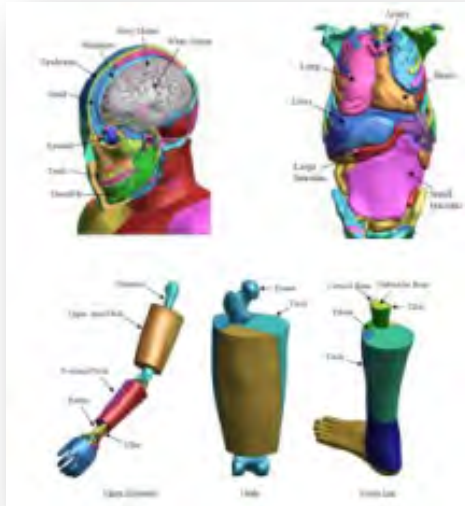
- Manage engineering teams with user authentication and administrative controls
- Data is secure every step of the way with end-to-end data encryption
- Jobs run on isolated, kernel-encrypted, private clusters
- Data centers include biometric entry authentication
- Platforms routinely submit to independent external security audits

Rescale maintains key relationships to provide LS-DYNA on demand on a global scale. If you have a need to accelerate the simulation process and be an innovative leader, contact Rescale or the following partners to begin running LS-DYNA on Rescale's industry-leading cloud simulation platform.

LSTC - DYNAmore GmbH JSOL Corporation

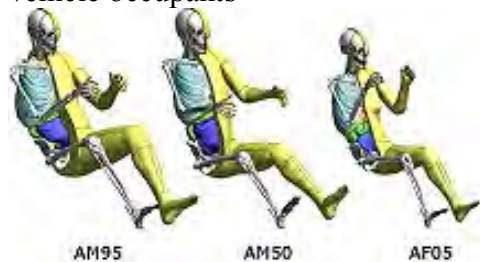
Rescale, Inc. - 1-855-737-2253 (1-855-RESCALE) - info@rescale.com - 944 Market St. #300, San Francisco, CA 94102 USA

TOYOTA - Total Human Model for Safety – THUMS

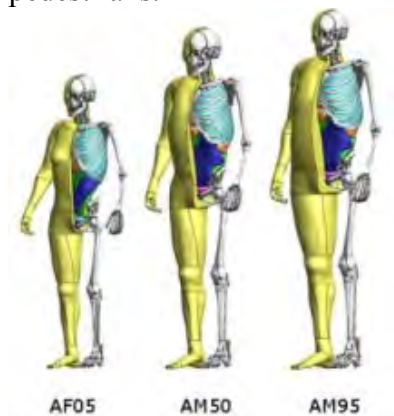


The Total Human Model for Safety, or THUMS®, is a joint development of Toyota Motor Corporation and Toyota Central R&D Labs. Unlike dummy models, which are simplified representation of humans, THUMS represents actual humans in detail, including the outer shape, but also bones, muscles, ligaments, tendons, and internal organs. Therefore, THUMS can be used in automotive crash simulations to identify safety problems and find their solutions.

Each of the different sized models is available as sitting model to represent vehicle occupants



and as standing model to represent pedestrians.



The internal organs were modeled based on high resolution CT-scans.

THUMS is limited to civilian use and may under no circumstances be used in military applications.

LSTC is the US distributor for THUMS.

Commercial and academic licenses are available.

For information please contact:

THUMS@lstc.com

THUMS®, is a registered trademark of Toyota Central R&D Labs.

LSTC – Dummy Models

LSTC Crash Test Dummies (ATD)

Meeting the need of their LS-DYNA users for an affordable crash test dummy (ATD), LSTC offers the LSTC developed dummies at no cost to LS-DYNA users.

LSTC continues development on the LSTC Dummy models with the help and support of their customers. Some of the models are joint developments with their partners.

e-mail to: atds@lstc.com

Models completed and available (in at least an alpha version)

- Hybrid III Rigid-FE Adults
- Hybrid III 50th percentile FAST
- Hybrid III 5th percentile detailed
- Hybrid III 50th percentile detailed
- Hybrid III 50th percentile standing
- EuroSID 2
- EuroSID 2re
- SID-IIs Revision D
- USSID
- Free Motion Headform
- Pedestrian Legform Impactors

Models In Development

- Hybrid III 95th percentile detailed
- Hybrid III 3-year-old
- Hybrid II
- WorldSID 50th percentile
- THOR NT FAST
- Ejection Mitigation Headform

Planned Models

- FAA Hybrid III
- FAST version of THOR NT
- FAST version of EuroSID 2
- FAST version of EuroSID 2re
- Pedestrian Headforms
- Q-Series Child Dummies
- FLEX-PLI

LSTC – Barrier Models

Meeting the need of their LS-DYNA users for affordable barrier models, LSTC offers the LSTC developed barrier models at no cost to LS-DYNA users.

LSTC offers several Offset Deformable Barrier (ODB) and Movable Deformable Barrier (MDB) models:

- ODB modeled with shell elements
- ODB modeled with solid elements
- ODB modeled with a combination of shell and solid elements
- MDB according to FMVSS 214 modeled with shell elements
- MDB according to FMVSS 214 modeled with solid elements

- MDB according to ECE R-95 modeled with shell elements
- AE-MDB modeled with shell elements

- IIHS MDB modeled with shell elements
- IIHS MDB modeled with solid elements
- RCAR bumper barrier

- RMDB modeled with shell and solid elements

e-mail to: atds@lstc.com.



FACEBOOK

[BETA CAE SYSTEMS SA](#)

[CADFEM](#)

[Cray Inc.](#)

[ESI Group](#)

[Lenovo](#)



TWITTER

[BETA CAE SYSTEMS SA](#)

[Cray Inc.](#)

[ESI Group](#)

[ETA](#)

[CADFEM](#)

[Lenovo](#)



LINKEDIN

[BETA CAE SYSTEMS SA](#)

[CADFEM](#)

[Cray Inc.](#)

[DYNAmore Nordic](#)

[ETA](#)

[Oasys](#)



NEWS FEEDS

[ETA:](#)



YOUTUBE Channel	WebSite URL
BETA CAE SYSTEMS SA	www.beta-cae.gr
CADFEM	www.cadfem.de
Cray Inc.	www.cray.com
ESI Group	www.esi-group.com
ETA	www.eta.com
Lancemore	www.lancemore.jp/index_en.html
Lenovo	

Publications Showcase

The following papers have been submitted so share with the engineering community.

All papers are copyright to the respective authors and companies and reprinted with permission

LS-DYNA® Smoothed Particle Galerkin (SPG) Method

Yong Guo C.T. Wu and Wei Hu

Livermore Software Technology Corporation, Livermore, CA, 94551 USA

LS-DYNA® Peridynamics for Brittle Fracture Analysis

Bo Ren, C. T Wu

Livermore Software Technology Corporation, Livermore, CA

E. Askari

Technical Fellow, Boeing Commercial Airplane, Seattle, WA

Best Fit and Its Application in Metal Forming

Xinhai Zhu, Li Zhang, Yuzhong Xiao

Livermore Software Technology Corporation, Livermore, CA

LS-DYNA[®] Smoothed Particle Galerkin (SPG) Method

Yong Guo¹, C.T. Wu² and Wei Hu³

¹Senior Scientist and Presenting Author, Livermore Software Technology Corporation,
7374 Las Positas Road, Livermore, CA, 94551 USA. Email: yguo@lstc.com

²Senior Scientist, Livermore Software Technology Corporation, 7374 Las Positas Road,
Livermore, CA, 94551 USA. Email: ctwu@lstc.com

³Scientist, Livermore Software Technology Corporation, 7374 Las Positas Road,
Livermore, CA, 94551 USA. Email: whu@lstc.com

Abstract: A new particle method for large inelastic deformation and material failure analyses from low to moderated high speed applications is presented. The new formulation is established following a meshfree Galerkin approach for a solving of partial differential equation in solid mechanics problem. A nonlocal strain field is introduced to the formulation via displacement smoothing which is shown to be related to the least-square stabilization method for the elimination of zero-energy modes, the enhancement of coercivity and the introduction of non-locality in the particle methods [1]. The discretized system of equation is consistently derived within the meshfree Galerkin variational framework [2] and integrated using a direct nodal integration scheme. As fully Lagrangian kernel is incapable of simulating the severe deformation and material separation problem, the updated-Lagrangian kernel and Eulerian kernel [3-5] are developed to reset the reference configuration, maintain the injective deformation mapping at the particles and naturally handle the material separation due to damage. Both SMP and MPP simulations are available in the released LS-DYNA[®] version. Several numerical benchmarks and industrial applications are provided in this presentation to demonstrate the effectiveness and accuracy of the new method.

Keywords: Meshfree method, nodal integration, stabilization, nonlinear

1 Introduction

Thanks for the characteristics of discretization flexibility and customized approximation, meshfree or particle methods have undergone extensive developments and led to widespread applications in interdisciplinary sciences and engineering over the past two decades. In particular, significant research efforts have been spent on the particle integration due to the conceptual simplicity and the reduced numerical restriction in modeling large deformation, moving discontinuity, and immersed problems in solid and structural applications.

Nevertheless, three types of instabilities [5] arise when a solid mechanics problem is solved by the particle method. Spurious energy mode in deformation is the first type of instabilities which mainly emanates from the rank instability [6] of the particle discrete

system. The rank instability is caused by the under-integration of weak forms inherent in the central difference formula from the direct particle integration scheme, and it requires numerical stabilization. Strain localization is driven by the material instability which presents the second type of instability in particle integration method. Physically, it is recognized [7] that the onset of strain localization in the rate-independent material coincides with the loss of ellipticity of the incremental problem. Mathematically, the strain localization leads to the ill-posedness of the incremental boundary value problem and requires a localization limiter [8]. Tension instability [9] is the third particle instability from discretization which results from the interaction of the second derivative of Eulerian kernel and the tensile stress [4]. Nowadays, the tensile instability can be entirely cured by an employment of Lagrangian kernels [10] in the solid mechanics applications.

So far, several stabilization techniques have been developed to remove the spurious energy modes in the meshfree nodal integration solution. The meshfree Galerkin/least-squares (GLS) stabilization approach [6] presents a reconstructed weak form where a bilinear term consisting of the residual of equilibrium equation is employed to stabilize the solution. The principle drawback of this residual stabilization approach is the contradictory demands on the stabilization control parameter placed by accuracy requirement. Wu *et al.* [1-2] developed the Smoothed Particle Galerkin (SPG) method in which a smoothed displacement field is introduced to stabilize the meshfree Galerkin nodal integration solution in large deformation and damage analyses. It was shown [3] that SPG method is closely related to the nonlocal meshfree method [8] by means of strain regularization analysis. Their analysis results reveal the SPG method is developed based on a fully nonlocal model in strain approximation and can be used for the large strain analysis. In this paper, the LS-DYNA[®] SPG method is introduced to the severe deformation and material failure simulation, several related LS-DYNA keywords and their descriptions are also provided.

Our paper is organized as follows. In the next section, an overview on SPG method is given. The corresponding LS-DYNA[®] SPG keywords are given in Section 3. Numerical examples are presented in Section 4 to illustrate the robustness and accuracy of the proposed method. Section 5 concludes with a brief summary.

2 Overview on SPG Method

The explicit dynamic equation of the SPG method is described by [1-3]

$$\mathbf{A}^{-T} \mathbf{M} \mathbf{A}^{-1} \ddot{\mathbf{U}} = \mathbf{A}^{-T} (\mathbf{f}^{ext} - \mathbf{f}^{int})$$

(1)

or equivalently

$$\mathbf{A}^{-T} \mathbf{M} \ddot{\mathbf{U}} = \mathbf{A}^{-T} (\mathbf{f}^{ext} - \mathbf{f}^{int})$$

(2)

where $\ddot{\mathbf{U}}$ and \mathbf{U} contains the vector of particle accelerations evaluated in the

smoothed nodal position system and generalized nodal position system, respectively. \mathbf{f}^{ext} and \mathbf{f}^{int} are corresponding external and internal force vectors, respectively. \mathbf{M} is the consistent mass matrix given by

$$\mathbf{M}_{IJ} = \mathring{\mathbf{a}} \sum_{N=1}^{NP} r_0 \Psi_I(\mathbf{X}_N) \Psi_J(\mathbf{X}_N) V_N^0 \mathbf{I} \quad (3)$$

where r_0 is the initial density, NP is the total number of particles, and $\Psi_I(\mathbf{X})$, $I=1, \dots, NP$ can be considered as the shape functions of the meshfree approximation for displacement field. V_K^0 denotes the initial volume of particle K . \mathbf{A} is a transformation matrix defined by

$$\mathbf{A}_{IJ} = \mathbf{f}_J(\mathbf{X}_I) \mathbf{I} = \mathring{\mathbf{a}} \sum_{K=1}^{NP} \Psi_K(\mathbf{X}_I) \Psi_J(\mathbf{X}_K) \mathbf{I} \quad (4)$$

Eq. (1) also can be rewritten as

$$\overline{\mathbf{M}} \ddot{\mathbf{U}} = \mathbf{A}^{-T} (\mathbf{f}^{ext} - \mathbf{f}^{int}) \quad (5)$$

with $\overline{\mathbf{M}} = \mathbf{A}^{-T} \mathbf{M} \mathbf{A}^{-1}$ defines a smoothed consist mass matrix. In explicit dynamic analysis a row-sum mass matrix is usually considered which is only computed once without involving matrix inversion at each time step. The smoothed consist mass matrix is now replaced by the row-sum mass matrix $\overline{\mathbf{M}}^{RS}$ to give

$$\overline{\mathbf{M}}_I^{RS} = \mathring{\mathbf{a}} \sum_J^{NP} \overline{\mathbf{M}}_{IJ} = \mathring{\mathbf{a}} \sum_J^{NP} \mathbf{A}_{IK}^{-T} \mathbf{M}_{KM} \mathbf{A}_{ML}^{-1} \quad (6)$$

As Lagrangian simulation proceeds, an updated Lagrangian/Eulerian kernel scheme is performed frequently to avoid the negative Jacobian in the Lagrangian calculation. In each adaptive step material quantities are computed at particles without the usage of background cells. Since the updated Lagrangian/Eulerian kernel approach does not involve remeshing and particle computation is evaluated node-wise, the material quantities at all particles are maintained in the Lagrangian setting and thus require no remap procedures. If we denote the variables before and after each adaptive time step to be superscripted with “-“ and “+“ respectively, the derivatives of material meshfree shape functions with respect to spatial coordinates right before $(k+1)$ -th adaptive time step can be expressed by

$$\Psi_{I,i}^-(\mathbf{x}^{k+1}) = \frac{\Psi_{I,i}^-(\mathbf{x}^{k+1})}{\mathbb{J}x_i^{k+1}} = \frac{\Psi_{I,i}^-(\mathbf{x}^{k+1})}{\mathbb{J}x_j^k} \frac{\mathbb{J}x_j^k}{\mathbb{J}x_j^{k+1}} = \frac{\Psi_{I,i}^-}{\mathbb{J}x_j^k} f_{ji}^{k-1} \quad (7)$$

where $f_{ji}^{k-1} = \frac{\mathbb{J}x_j^k}{\mathbb{J}x_j^{k+1}}$ defines the inverse of incremental deformation gradient from k -th

adaptive time step. At $(k+1)$ -th adaptive time step, the new derivatives of material meshfree shape functions becomes

$$\psi_{i,i}^+(\mathbf{x}^{k+1}) = \frac{\prod \psi_i^+(\mathbf{x}^{k+1})}{\prod x_i} \quad (8)$$

Since no remap procedures are considered in the adaptive step, the particle mass is taken to be the same during the explicit dynamics analysis. The current particle volume required for the calculation of internal force is updated according to the continuity equation given by

$$V_I = \frac{r_0}{r_I} V_I^0 \quad (9)$$

$$\frac{dr_I}{dt} = -r_I \tilde{\mathbf{N}} \times (\dot{\mathbf{u}}_I) = -r_I \mathbf{a} \cdot \dot{\mathbf{u}}_I \times \psi_{J,x}(\mathbf{x}_I) \quad (10)$$

In LS-DYNA[®], we consider the adaptive step be periodically taken by a constant time interval. Figure 1 illustrates the evolution of updated Lagrangian/Eulerian kernel in one adaptive step.

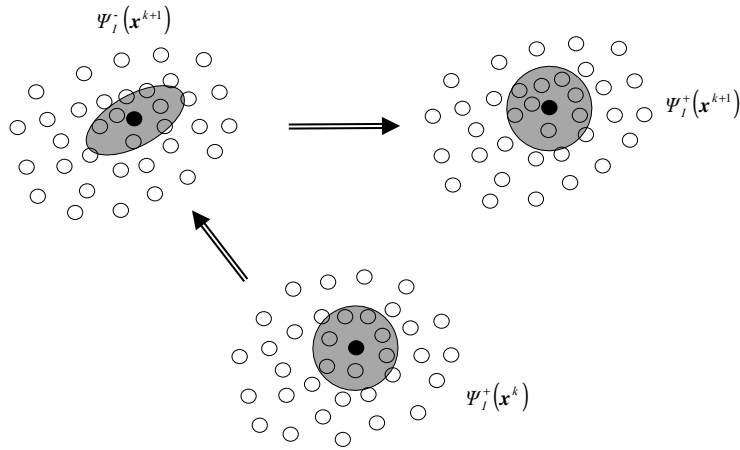


Figure 1. The evolution of updated Lagrangian/Eulerian kernel in the adaptive scheme.

3 LS-DYNA[®] SPG Keywords

The SPG method is activated with *SECTION_SOLID_{SPG} keyword card and the element formulation is 47.

*SECTION_SOLID_{SPG}

Card1	1	2	3	4	5	6	7	8
Variable	SECID	ELFORM	AET					
Type	I	47	I					

Default								
---------	--	--	--	--	--	--	--	--

Card 2 is required for additional parameters for SPG method and Card 3 is required for damage and failure analysis.

Card2	1	2	3	4	5	6	7	8
Variable	DX	DY	DZ	ISPLINE	KERNEL	LSCALE	SMSTEP	SWTIME
Type	F	F	F	I	I	F	I	F
Default	1.5	1.5	1.5	0	3		15	
Card3	1	2	3	4	5	6	7	8
Variable	IDAM	FS	STRETCH					
Type	I	F	F					
Default	0		1.2					

The variable description is as following:

<u>VARIABLE</u>	<u>DESCRIPTION</u>
SECID	Section ID.
ELFORM	Element formulation options. Set to 47 to active SPG method.
DX, DY, DZ	Normalized dilation parameters of the kernel functions in X, Y and Z directions.
ISPLINE	Option for kernel functions. EQ.0: Cubic spline function (default). EQ.1: Quadratic spline function. EQ.2: Cubic spline function with circular shape.
KERNEL	Type of kernel approximation. EQ.0: updated Lagrangian kernel. EQ.1: Eulerian kernel. EQ.2: Semi-Lagrangian kernel. EQ.3: Pseudo-Lagrangian kernel.
LSCALE	Not used.

SMSTEP	Interval of time steps to conduct displacement regularization.
SWTIME	Time to switch from updated Lagrangian kernel to Eulerian kernel.
IDAM	Damage option. EQ.0: Continuum damage mechanics (default) EQ.1: Phenomenological strain damage EQ.2: Maximum principal strain damage
FS	Failure strain if IDAM=1; maximum principal strain if IDAM=2
STRETCH	Stretching parameter if IDAM=1

In order to display the SPG part as particles in LS-PREPOST, one can follow the steps below:

- (1) In the “Set Part Appearance” panel (“Appear”), choose “Grid” and “Sphere” options and click on SPG part, the SPG nodes will be shown as grid points.
- (2) In the “Set Display Options” panel (“Setting”), choose “SPH/Particle” and set “Radius Scale”, “Sphere divs” and “Style” options. Apply your settings by click “Aply” button.
- (3) Go to “Fringe Component” panel (“Fcomp”) and draw the contour. The SPG part will be shown as particles.

4 Numerical Examples

4.1 Material failure simulation in a 3D plate

To demonstrate the applicability of SPG in the general three-dimensional problem, the material failure of a metal plate is simulated. The 3D metal plate has a size of 0.2m in diameter and 0.023m in thickness. It is subjected to an indentation of ball with a size of 0.03m in diameter. The ball is assumed to be rigid and is traveling at a constant speed of 0.893m/s. The material constants of the metal bar are [12]: Young’s modulus $E=206.9$ GPa, Poisson’s ratio $\nu=0.29$, density $\rho^0=7860$ kg/m³ and the isotropic hardening rule $s_y(\bar{e}^p) = s_y^0 + a\bar{e}^p + (s_y^* - s_y^0)(1 - e^{-b\bar{e}^p})$ with coefficients $\beta=16.93$, $s_y^0=0.45$ GPa, $s_y^* = 0.715$ GPa and $a = 0.12924$ GPa. The 3D plate is discretized by the finite element analysis model which is composed of 35470 hexahedra elements (39941 nodes) as shown in Figure 2. To study the effect of material failure in the simulation, the Eulerian

kernel is adopted (KERNEL=1) and failure criteria (IDAM=1 and fs=1.0) is considered.

The progressive deformed geometries are plotted in Figures 3 (a) and (b) for the top view and bottom view, respectively. For this low speed application, no debris is observed in the metal plate. The ball penetrates the metal plate with desired multiple radiating star-like cracks. Figure 4 presents the load-displacement response in which the contact force reduces to zero when the ball is fully penetrating the metal plate.

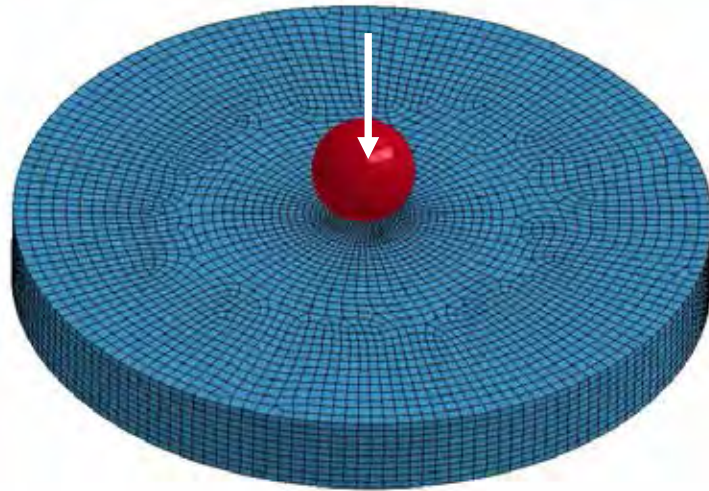


Figure 2. The finite element mesh of 3D metal plate in material failure problem.

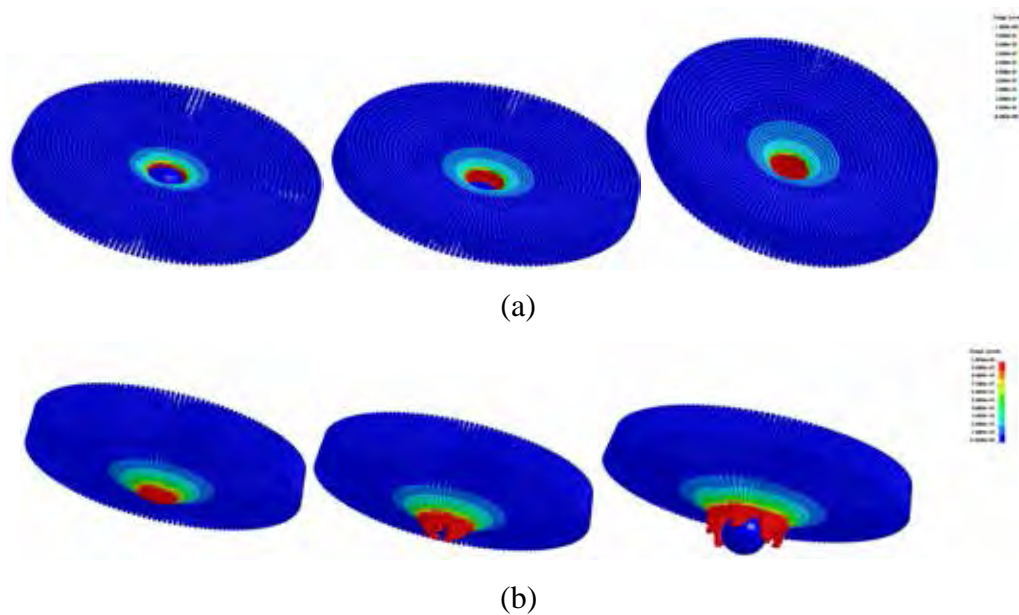


Figure 3. Deformed configuration of 3D plate in effective plastic strain contour: (a) top view; (b) bottom view.

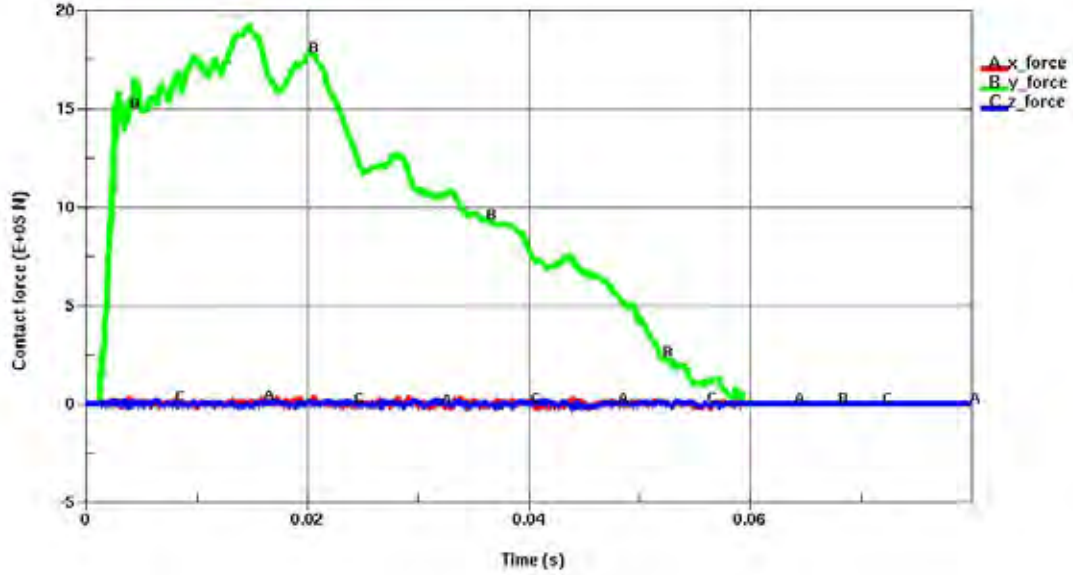


Figure 4. Force response of the contact force in failure simulation.

4.2. 3D metal grooving simulation

This problem is studied to identify the applicability of SPG method in three-dimensional severe deformation analysis. A metal block of size $0.1 \text{ m} \times 0.06 \text{ m} \times 0.02 \text{ m}$ is fixed at the bottom and grooved by a rigid rotating roller as shown in Figure 5. The width of the roller is 0.008 m . The roller has a constant rotating speed $\omega=125 \text{ rad/s}$ and is traveling at a transverse speed $V=0.5 \text{ m/s}$. For present purpose, we further assume the grooving process is isothermal and frictional coefficient for the contact between roller and work piece is 0.1 . The material has an initial density $\rho^0 = 2700 \text{ kg/m}^3$. The strain-hardening elastic-plastic material properties are: Young's modulus $E=70.0 \text{ GPa}$, Poisson's ratio $\nu=0.3$, and an isotropic hardening rule $\mathbf{s}_y(\bar{\epsilon}^p) = \mathbf{s}_y^0 + \mathcal{G}E_p \bar{\epsilon}^p$ with coefficients $\gamma=1.0$, $\mathbf{s}_y^0=0.1 \text{ GPa}$, and $E_p=1.5\text{e-}2 \text{ GPa}$. The finite element analysis model for the work piece contains 15000 hexahedra elements (17391 nodes) which are uniformly distributed as shown in Figure 5. For finite element methods, both one-point integration with hourglass control formulation (FEM1) and selective reduced integration formulation (FEM2) are considered for the comparison. Explicit dynamics analysis is conducted for this simulation.

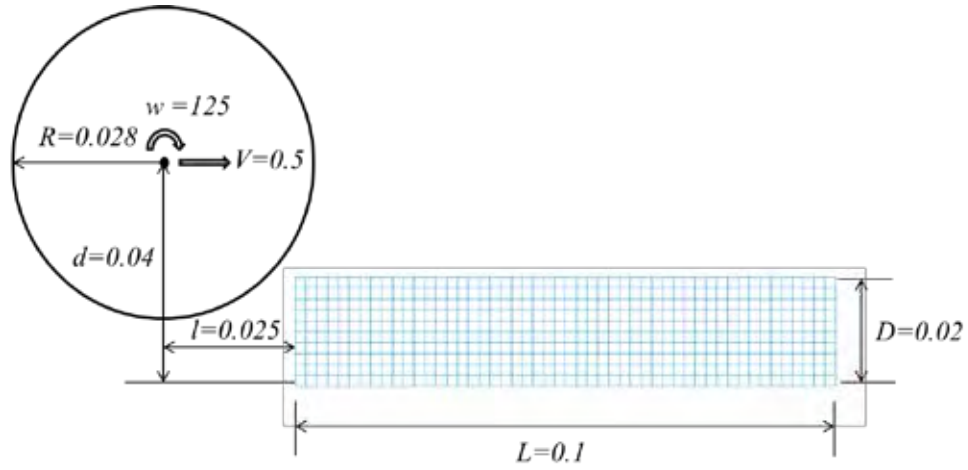
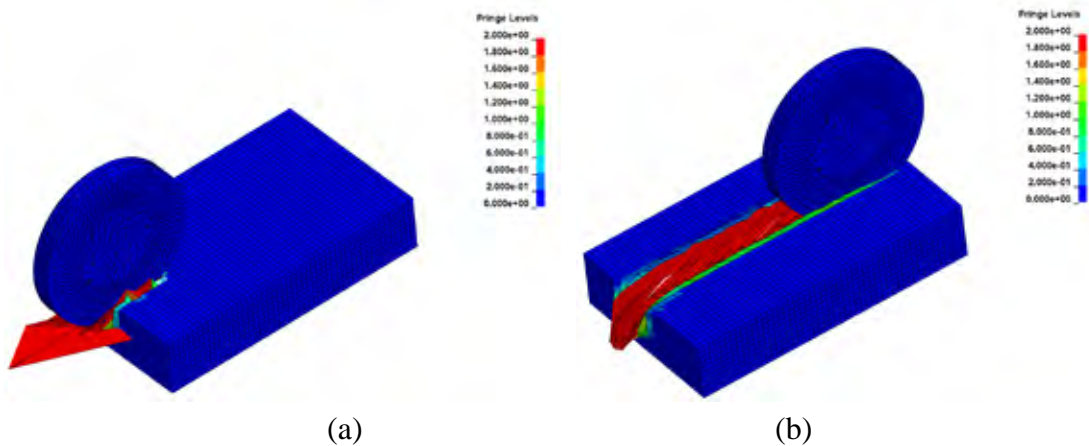
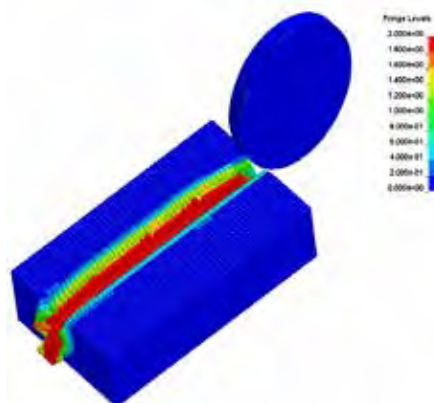


Figure 5. 3D metal grooving problem.

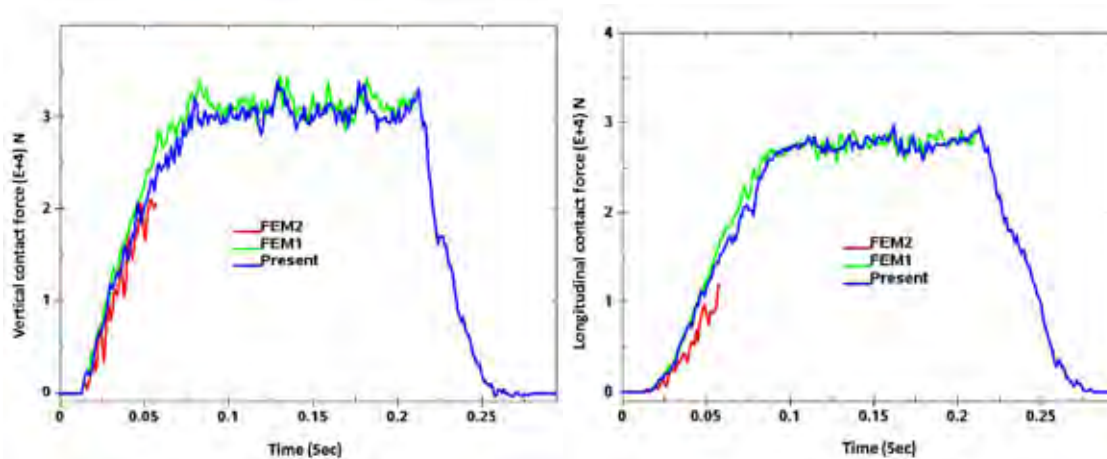
The final deformed geometries with effective plastic strain contours are plotted in Figures 6 (a)-(c) for the FEM2, FEM1 and SPG method, respectively. As shown in Figure 6 (a), FEM2 method experiences severe mesh distortion problem and the simulation stops in the early stage. Surprisingly, the FEM1 method improves the simulation in FEM2 and completes two-thirds of the simulation in grooving process as shown in Figure 6 (b). On the other hand, the SPG method is able to accomplish the grooving simulation as depicted in Figure 6 (c) for the final deformed geometry. It is worthwhile to note that the SPG method is very stable and no shooting nodes are observed in the simulation. The comparisons of contact force in vertical and longitudinal directions are given in Figures 7 (a) and (b), respectively. Good agreement between FEM1 solution and the SPG solution is shown in the plunging phase and steady state of the grooving phase before roller retracts. In contrast, the negative volume causes the FEM2 simulation to abort early in the plunging phase as shown in the contact force response.





(c)

Figure 6. Final deformation in the grooving problem: (a) FEM2; (b) FEM1; and (c) present method.



(a)

(b)

Figure 7. Comparison of contact force in the grooving problem: (a) vertical direction; and (b) longitudinal direction.

To study the effect of material failure in grooving simulation, the Eulerian kernel is adopted (KERNEL=1) and failure criteria (IDAM=1 and fs=0.3) is considered. The final deformed geometry with effective plastic strain contours are plotted in Figures 8 (a) and (b) for the SPG method without and with material failure, respectively. The maximum range of the effective plastic strain contour plot in Figure 8 is 0.3. Apparently, the influence region of effective plastic strain in the case of damage model is more profound than that of non-damage model. The difference can be verified on their contact force responses as shown in Figures 9 (a) and (b) for the vertical and longitudinal directions, respectively. As shown in Figure 9, the contact forces in both vertical and longitudinal directions reduce in the damage case particularly during the steady state of the grooving process. The reduction of contact force response in the longitudinal direction is more evident than the vertical direction. This is due to the potential loss of frictional contact caused by the material failure on the grooving

surface.

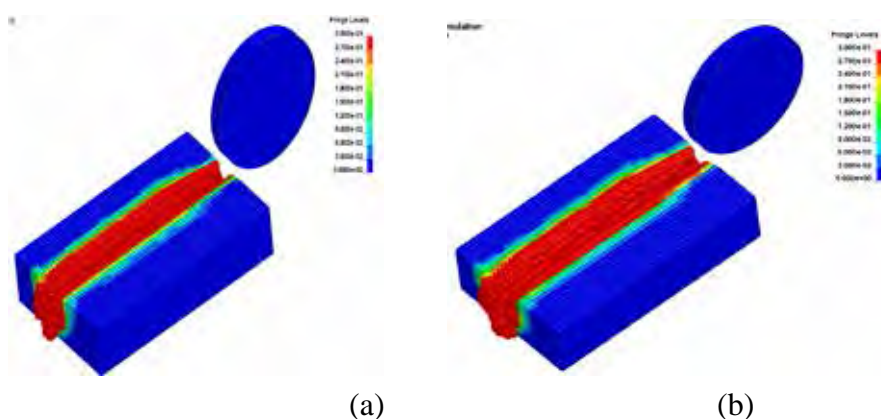


Figure 8. Final deformation in the SPG grooving simulation: (a) non-damage; and (b) damage.

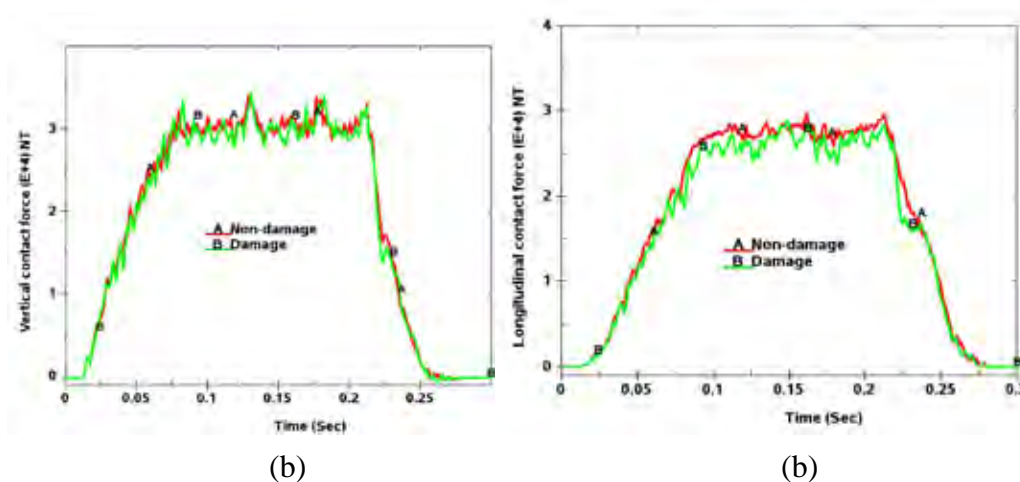


Figure 9. Comparison of contact force in the SPG grooving simulation: (a) vertical direction; and (b) longitudinal direction.

5 Conclusion

A stable and accurate particle method is attractive from the viewpoint of formulation simplicity and simulation capability in the nonlinear analysis of solid mechanics problems. In this paper, the LS-DYNA[®] SPG method is introduced which is free from stabilization control parameters and integration cells for the particle computation. Several kernel formulations have been incorporated into the nonlinear SPG formulation to enhance the simulation capability for severe deformation and damage analysis in ductile materials. The SPG method can be considered as an alternative method in LS-DYNA[®] to model various manufacturing and crashworthiness problems that require a consideration of material failure.

- [1] Wu C.T., Guo Y., Hu W. An introduction to the LS-DYNA smoothed particle Galerkin method for severe deformation and failure analysis in solids. 13th International LS-DYNA Users Conference, Detroit, MI, June 8-10, 1-20, 2014.
- [2] Wu C.T., Hu W., Koishi M. (2015) A smoothed particle Galerkin formulation for extreme material flow analysis in bulk forming applications. *International Journal of Computational Methods*, Accepted for publication.
- [3] Wu C.T., Koishi M., Hu W. (2015) A displacement smoothing induced strain gradient stabilization for the meshfree Galerkin nodal integration method. *Computational Mechanics*, Vol. 56 (1), pp. 19-37.
- [4] Wu C.T., Wang D.D., Guo Y. (2015) An immersed particle modeling technique for the three-dimensional large strain simulation of particulate-reinforced metal-matrix composites, *Applied Mathematical Modelling*, DOI: 10.1016/j.apm.2015.09.107, in press.
- [5] Belytschko T., Guo Y, Liu, W.K, Xiao S.P. (2000) A unified stability analysis of meshless particle methods. *International for Numerical Methods in Engineering*, Vol. 48, pp. 1359-1400.
- [6] Beissel S., Belytschko T. (1996) Nodal integration of the element-free Galerkin method. *Computer Methods in Applied Mechanics and Engineering* Vol. 139, pp. 49-74.
- [7] Hill R. (1962) Acceleration waves in solids. *Journal of Mechics and Physics of Solids*, Vol. 10, pp. 1-16.
- [8] Chen J.S., Wu C.T., Belytschko T. (2000) Regularization of material instabilities by meshfree approximations with intrinsic length scales. *International for Numerical Methods in Engineering*, Vol. 47, pp. 1303-1322.
- [9] Dyka, C.T., Randles P.W., Ingel R.P., (1997) Stress points for tension instability in SPH, *International for Numerical Methods in Engineering* Vol. 40, pp.2325-2341.
- [10] Belytschko T., Guo Y., Liu W.K., Xiao S.P. (2000) A unified stability analysis of meshless particle methods. *International for Numerical Methods in Engineering* Vol. 48, pp. 1359-1400.

LS-DYNA[®] Peridynamics for Brittle Fracture Analysis

Bo Ren¹, C. T Wu^{2*} and E. Askari³

¹ Scientist, Livermore Software Technology Corporation, 7374 Las Positas Road, Livermore, CA 94551 e-mail: boren@lstc.com

^{2*} Senior Scientist and Presenter, Livermore Software Technology Corporation, 7374 Las Positas Road, Livermore, CA 94551 e-mail: ctwu@lstc.com

³ Technical Fellow, Boeing Commercial Airplane, Seattle, WA 98124 e-mail: abe.askari@boeing.com

Abstract

Peridynamics is a new nonlocal theory that provides the ability to include displacement discontinuities in a continuum body without explicitly modelling the crack surface. In comparison to the classical weakly nonlocal or strictly nonlocal models, the peridynamics equation of motion is free of spatial derivative of displacement. The peridynamics also does not require sophisticated book keeping of degrees of freedom or jump conditions in tracking the moving discontinuities. Those features of peridynamics offer significant advantages over other advanced numerical methods for the brittle fracture analysis particularly in three-dimensional problems.

The explicit dynamics version of bond-based peridynamics model has been implemented in LS-DYNA[®] using the Discontinuous Galerkin (DG) finite element approach to enforce the boundary conditions, constraints, contacts as well as to handle the non-uniform mesh in the engineering practice. The classic material parameters, such as elastic modulus and fracture energy release rate are employed for the determination of material response and failure in brittle material. The LS-DYNA[®] Peridynamics supports 8, 6 and 4-noded solid elements with the ability to handle multiple and branching cracks. Several numerical benchmarks are utilized to demonstrate the effectiveness and accuracy of the LS-DYNA[®] peridynamics in brittle fracture analysis.

Key Words: Bond-Based Peridynamics, Discontinuous Galerkin, Finite Element Method, Meshfree Method

1. Introduction

The numerical simulation of material failure is a longstanding challenge in the computational mechanics society as well as in the industry. The main difficulty arises from the incompatibility between the existing physical discontinuities emerging from material failure and the partial differential equations utilized by the classic continuum mechanics theory to describe the deformation of a solid. Another numerical difficulty of the material failure simulation in solids is the challenge of maintaining an adequate data structure representing the evolving crack surfaces during the dynamic process. Much effort has been devoted to overcome these numerical challenges. At the continuum level, the XFEM method [1] introduces the level set method into the finite elements and implicitly determines the position and orientation of crack tips. However, as a mesh-based method, a sophisticated book-keeping algorithm is required to track the crack surface which turns out to be very difficult in 3D problems. The Cohesive FEM [2] method can naturally represent the evolving discontinuity in computational domain. However, cohesive laws in the cohesive model are phenomenological which not only ruins the consistency of the material property field but also leads to a convergence problem even in the isotropic solid state. The meshfree methods [3] also have been developed to model the material failure. Compared to the XFEM, the meshfree methods update the connectivity with customized approximations and represent the moving boundary conditions with less effort. However, the current techniques to handle multiple cracks seem to not be robust requiring further research. On the other hand to avoid the localization problem and thus the mesh sensitivity issue, the nonlocal theories which have been proposed since the late of 1970s [4] are used in XFEM and meshfree methods. To evade the spatial differential operation nearby crack surface, the continuum weakly or strictly nonlocal models [5] have been developed. This leads to a

formulation where the spatial derivatives appearing in the weak form of corresponding partial differential equations are smeared along the material failure surfaces.

Peridynamics is one of the nonlocal methods proposed by Silling [6,7]. It has been considered as a viable and efficient numerical method for the material and structural failure problems. Peridynamics theory replaces the spatial differential term in the classical mechanical theories by a nonlocal integral term that assembles the interaction forces of a material point. The first peridynamics model was presented in 1997. It was named bond-based peridynamics and was applied to the brittle materials [6]. In the bond-based peridynamics model, each material point interacts with its neighbors in a compact zone. The interaction between two material points is called a “bond” which is independent from other bonds. The pair-wise bond forces are collinear with the line connecting these two material points and have opposite directions. The bond-based peridynamics model is well-developed and has been applied to the simulation of damage and fracture processes in brittle materials [8], reinforced concrete materials [9], composite laminate structures [10], brazed joints [11] and geo-materials [12]. The three-dimensional formulas of bond-based peridynamics can be derived from a pair-wise elastic potential which shall result in a constant Poisson’s ratio $\nu = 0.25$ rooted in the so-called Cauchy relation, i.e., the elastic modulus tensor satisfies the relations as $D_{1122} = D_{1212}$. To address this restriction, the so-called ordinary and non-ordinary state-based peridynamics models [13,14] were proposed in which the bond forces are independent each other in contrast with that in bond-based peridynamics. The state-based peridynamics evaluates the bond force based on the multi-body potential which has the capability to represent both the changing of volume and shear effect. Although the state-based peridynamics model has the potential to solve the general material failure problems, there are still some technical issues [15, 16] which need to be addressed and resolved before it is implemented in LS-DYNA®.

The motivation of the peridynamics development is the prediction of material damage in a 3D solid. Thus the peridynamics computational space is firstly discretized by a set of

material particles. Consequently, the nonlocal integral term of peridynamics theory is implemented by the nodal integral method [17]. This meshfree type of implementation can capture the crack path without numerical limitations. However, the boundary condition enforcement cannot follow the standard way as that in the meshfree Galerkin formulation. Another shortcoming is that the accuracy of computation decays dramatically in the case of non-uniform discretization. An alternative way to perform the spatial integration and avoid those numerical defects in peridynamics models is constructing an approximation field of the kinematic quantity by finite element (FE) shape function [18, 19]. Based on this argument, the integration operations can be carried out through Gaussian integration points. Several studies [20, 21] have been conducted to verify that the peridynamics model can be implemented in the FEM framework with nonlocal boundary conditions. The FEM peridynamics inherits the advantages of FEM method such as the straightforward boundary condition enforcement and convergence with non-uniform discretization. But the regular FEM method based on Galerkin weak form has a continuous computational domain which violates the original motivation of peridynamics. To represent the strong discontinuities in FEM peridynamics, the continuous approximation field can be replaced by a piece wise continuous field which results in a discontinuous Galerkin formula for peridynamics [19, 22, 23]. The piece-wise continuous approximation implies the capability to represent the crack surfaces automatically. The research results [22, 23] indicate that this model can lead to a stable solution for dynamic problems as well as quasi-static problems by FEM peridynamics models.

This paper presents a FEM implementation of the bond-based peridynamics model in LS-DYNA® which is practically convenient to those who are interested in the brittle fracture analysis. The LS-DYNA® peridynamics converts the nonlocal quantities in peridynamics model to the equivalent continuous quantities. The LS-DYNA® users with experiences of using classic FEM can easily handle peridynamics model as that of the continuum models. In section 2, the basic bond-based peridynamics formulations are

reviewed. Section 3 constructs the discontinuous Galerkin weak form for the bond-based peridynamics model. Then the relations between the nonlocal peridynamics quantities and classic mechanics quantities are derived based on the equivalent elastic energy density in Section 4. Section 5 introduces the LS-DYNA® keywords to deploy the peridynamics computation. After that, several benchmark problems are presented in Section 6. Final remarks are given in Section 7.

2. The bond-based peridynamics model

The bond-based peridynamics model can be considered a macro-scale molecular dynamics model. The dynamic motion of a peridynamics point is governed by the collective of the interaction forces between this point and its neighboring points in a compact zone. The equation of motion of any point (\mathbf{X}) at reference configuration at time t is:

$$\rho \ddot{\mathbf{u}} = \int_{H_{\mathbf{X}}} \mathbf{f}(\mathbf{u}(\mathbf{X}', t) - \mathbf{u}(\mathbf{X}, t), \boldsymbol{\xi}) dV_{\mathbf{X}'} + \mathbf{b}(\mathbf{X}, t), \quad (1)$$

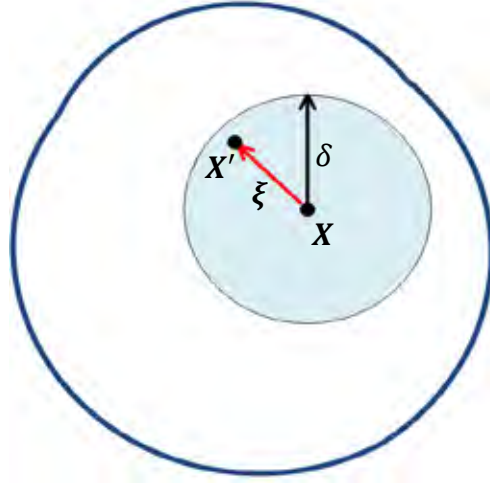
where $H_{\mathbf{X}}$ is a compact neighborhood zone of \mathbf{X} , named as horizon. The horizon of \mathbf{X} is defined as $H_{\mathbf{X}} = \{\mathbf{X}' \mid |\mathbf{X}' - \mathbf{X}| \leq \delta\}$, where δ is the radius of a sphere centered at \mathbf{X} . $\boldsymbol{\xi}$ denotes a bond as $\boldsymbol{\xi} = \mathbf{X}' - \mathbf{X}$. The pair of interaction forces (\mathbf{f}) between \mathbf{X} and \mathbf{X}' is collinear with the bond and has opposite orientation which is determined by the relative displacement of two points: $\boldsymbol{\eta} = \mathbf{u}(\mathbf{X}', t) - \mathbf{u}(\mathbf{X}, t)$. \mathbf{b} is the prescribed body force density. The integration term in Eq. (1) collects all the bond forces imposed to \mathbf{X} .

There are two import hypothesizes of the bond force: (1) the bond force is a short range force, i.e., it only appears inside the compact zone:

$$\mathbf{f}(\boldsymbol{\eta}, \boldsymbol{\xi}) = 0 \text{ when } |\boldsymbol{\xi}| > \delta. \quad (2)$$

(2) \mathbf{f} is a pairwise interaction force satisfying:

$$\mathbf{f}(-\boldsymbol{\eta}, -\boldsymbol{\xi}) = -\mathbf{f}(\boldsymbol{\eta}, \boldsymbol{\xi}), \quad (3)$$



which ensures the conservation of linear momentum [14].

Fig. 1 the peridynamics model

In the bond-based peridynamics model, the material is considered as *microelastic* that implies a bond force is derivable from a *micropotential* w :

$$\mathbf{f}(\boldsymbol{\eta}, \boldsymbol{\xi}) = \frac{\partial w(\boldsymbol{\eta}, \boldsymbol{\xi})}{\partial \boldsymbol{\eta}}, \quad (4)$$

where the *micropotential* is a peridynamics concept which is a measurement of the elastic energy stored in a bond. In contrast to that of classic continuous mechanics, the *micropotential* has the unit of N/m^5 . Consequently, the bond force $\mathbf{f}(\boldsymbol{\eta}, \boldsymbol{\xi})$ has the dimension of N/m^6 . The energy density of point \mathbf{X} can be collected through all bonds connecting to it:

$$W = \frac{1}{2} \int_{H_X} w(\boldsymbol{\eta}, \boldsymbol{\xi}) dV_{X'}. \quad (5)$$

The governing equation of bond-based peridynamics is constructed based on the derivative of energy equation. Here the formations of $w(\boldsymbol{\eta}, \boldsymbol{\xi})$ represent the material types. It can be linear, non-linear isotropic or anisotropic materials. The current LS-DYNA® implementation employs the *prototype microelastic brittle* (PMB) material model [15]. The PMB model is a linear isotropic material model in which each bond is considered as a linear spring. The *micropotential* of a PMB bond is evaluated from the stretch of bond:

$$w(|\boldsymbol{\eta}|, |\boldsymbol{\xi}|) = \frac{1}{2} c s^2 |\boldsymbol{\xi}|, \quad (6)$$

where c is the spring constant named as *microelastic* modulus. s is the bond stretch ratio:

$$s = \frac{|\boldsymbol{\xi} + \boldsymbol{\eta}| - |\boldsymbol{\xi}|}{|\boldsymbol{\xi}|}. \quad (7)$$

In the case of small deformation, the bond force is calculated as:

$$\mathbf{f}(\boldsymbol{\eta}, \boldsymbol{\xi}) = c s \frac{\boldsymbol{\xi}}{|\boldsymbol{\xi}|} \quad (8)$$

The bond-based peridynamics model captures the material failure by a bond-based failure criterion: the critical bond stretch (s_c) [14, 15]. With this failure model, a bond with stretch above s_c will be broken and this breakage is irreversible. It is said that a crack surface will be formed when all bonds crossing this surface are broken. Under this hypothesis, the critical stretch is related to classic fracture mechanics quantity: energy release rate, G_c [14, 15]. In the 3D case, this relation is given as:

$$G_c = \frac{\pi c s_c^2 \delta^5}{10}. \quad (9)$$

Unlike the local damage mechanics models, there is no explicit damage indicator in the peridynamics model. The failure is introduced at the bond level which is a nonlocal status. However, a local damage indicator of a point can be defined through the status of bonds [14, 15]:

$$D(\mathbf{X}) = 1 - \frac{\int_{H_X} \varphi(\boldsymbol{\xi}) dV_{\mathbf{X}'}}{\int_{H_X} dV_{\mathbf{X}'}} \quad (10)$$

where:

$$\varphi(\boldsymbol{\xi}) = \begin{cases} 1, & \text{for } s(\boldsymbol{\xi}) < s_c \\ 0, & \text{otherwise} \end{cases} \quad (11)$$

3. The Discontinuous Galerkin weak form

The computational domain of a peridynamics problem is denoted as Ω with essential boundary condition S_u . The solution of this problem is located in a subspace of Banach space: $S(\Omega) = \{\mathbf{u}(\mathbf{X}) \in L^2(\Omega) | \mathbf{u}(\mathbf{X}_g) = g(\mathbf{X}_g) \forall \mathbf{X}_g \in S_u\}$. Let $\mathbf{v}(\mathbf{X})$ denote a test function located at $S'(\Omega) = \{\mathbf{v}(\mathbf{X}) \in L^2(\Omega) | \mathbf{v}(\mathbf{X}_g) = \mathbf{0} \forall \mathbf{X}_g \in S_u\}$. The Galerkin weak form of problem of Eq. (1) is posed as:

$$\int_{\Omega} \rho \dot{\mathbf{u}}(\mathbf{X}) \cdot \mathbf{v}(\mathbf{X}) dV_{\mathbf{X}} = \int_{\Omega} \int_{H_{\mathbf{X}}} \mathbf{f}(\boldsymbol{\eta}, \boldsymbol{\xi}) dV_{\mathbf{X}'} \cdot \mathbf{v}(\mathbf{X}) dV_{\mathbf{X}} + \int_{\Omega} \mathbf{b}(\mathbf{X}) \cdot \mathbf{v}(\mathbf{X}) dV_{\mathbf{X}}$$

$$\forall \mathbf{u}(\mathbf{X}) \in S(\Omega), \mathbf{v}(\mathbf{X}) \in S'(\Omega). \quad (12)$$

Like the regular FEM method based on the continuous Galerkin method, the approximation fields of the solution ($\mathbf{u}(\mathbf{X})$) and test function ($\mathbf{v}(\mathbf{X})$) are constructed based on the FEM shape function:

$$u_i(\mathbf{X}) = u_i^A N^A(\mathbf{X}), \quad v_i(\mathbf{X}) = v_i^B N^B(\mathbf{X}), \quad (13)$$

where the subscript i indicates the dimensional index and upper capital A and B denote the node indexes in an element, i.e., u_i^A denotes the displacement u_i of node A. Based on Eq.(13), the Eq. (12) can be organized in the component form:

$$\int_{\Omega} \rho \dot{u}_i^A N^A(\mathbf{X}) N^B(\mathbf{X}) dV_{\mathbf{X}} = \int_{\Omega} \left(\int_{H_{\mathbf{X}}} f_i(\boldsymbol{\eta}, \boldsymbol{\xi}) dV_{\mathbf{X}'} \right) N^B(\mathbf{X}) dV_{\mathbf{X}} + \int_{\Omega} b_i(\mathbf{X}) N^B(\mathbf{X}) dV_{\mathbf{X}}. \quad (14)$$

In the discretization of the continuous FEM domain, the adjacent elements share nodes whereas each element has its own nodes in discontinuous FEM domain, i.e., the total nodal number equals the total element number times the node number in one elements. Eq. (14) contains two levels of integration. The first level of integration is the computational domain integration discretized by the summation of Gaussian points like the regular FEM integration:

$$\begin{aligned}
& \sum_{g=1}^{ng} \rho N^B(\mathbf{X}^g) \Delta V^g \ddot{u}_i^A = \\
& \sum_{g=1}^{ng} \left(\int_{H_X} f_i(\boldsymbol{\eta}(\mathbf{X}^g), \boldsymbol{\xi}(\mathbf{X}^g)) dV_{X'} \right) N^B(\mathbf{X}^g) \Delta V^g + \\
& \sum_{g=1}^{ng} b_i(\mathbf{X}) N^B(\mathbf{X}^g) \Delta V^g,
\end{aligned} \tag{15}$$

where ng denotes the total number of Gaussian points in the domain. The row-sum mass matrix treatment is used in the left side of Eq. (15) for the explicit dynamic simulation. The integration remaining in Eq. (15) represents the nonlocal effect of a Gaussian point \mathbf{X}^g . Because the first level of integration is carried out through Gaussian points, the bond connectivity in the domain is build up based on the Gaussian points system. This treatment leads to:

$$\begin{cases} \boldsymbol{\xi}(\mathbf{X}^g) = N^A(\mathbf{X}^g) \mathbf{X}^A - N^{A'}(\mathbf{X}^{g'}) \mathbf{X}^{A'} \\ \boldsymbol{\eta}(\mathbf{X}^g) = N^A(\mathbf{X}^g) \mathbf{u}^A - N^{A'}(\mathbf{X}^{g'}) \mathbf{u}^{A'} \end{cases} \tag{16}$$

where $\boldsymbol{\xi}(\mathbf{X}^g)$ is a bond linking Gaussian point \mathbf{X}^g and its neighbor $\mathbf{X}^{g'}$ in its horizon that is a Gaussian point either. Therefore the integration domain in Eq. (15) which is a sphere centered at \mathbf{X}^g can be discretized by Gaussian points. Finally the discretized bond-based peridynamics governing equation becomes:

$$\begin{aligned}
& \sum_{g=1}^{ng} \rho N^B(\mathbf{X}^g) \Delta V^g \ddot{u}_i^A = \sum_{g=1}^{ng} \left(\sum_{g'=1}^{ng'} f_i(\boldsymbol{\eta}(\mathbf{X}^g, \mathbf{X}^{g'}), \boldsymbol{\xi}(\mathbf{X}^g, \mathbf{X}^{g'})) \Delta V^{g'} \right) N^B(\mathbf{X}^g) \Delta V^g + \\
& \sum_{g=1}^{ng} b_i(\mathbf{X}^g) N^B(\mathbf{X}^g) \Delta V^g,
\end{aligned} \tag{17}$$

where ng' is the total number of neighbors of Gaussian point \mathbf{X}^g . $\mathbf{X}^{g'}$ can exist crossing elements. The discontinuous Galerkin weak form with classic constitutive model requires a flux function to transform momentum between adjacent elements [22]. The advantage of this working is that the nonlocal bond forces, i.e., the nonlocal constitutive law, Eq. (8) ensures a continuum body even the approximation field is piecewise continuum. Because the approximation field is constructed by regular FEM shape function, the boundary

conditions can be enforced by the standard FEM way. The boundary effect of the nonlocal constitutive law will be corrected in the sense of equivalent elastic energy density throughout the domain and as further described in the next section.

4. The equivalent classic mechanics quantities for PMB material

As discussed in Section 2, there are only two material quantities which characterize a PMB material: the microelastic modulus c and the critical bond stretch s_c . Both of these two quantities are not ordinary material constants used in the classic mechanics models, such as elastic modulus and Poisson's ratio. Fortunately, the microelastic modulus and critical bond stretch can be related to classic mechanics quantities based on the equivalent strain energy in the continuous mechanics sense. It's known that the Poisson's ratio of a PMB is restricted to 0.25 in 3D case. In this work, the microelastic modulus c is calculated to enforce an equivalent elastic energy density in PMB.

The classic elastic energy density inside a solid under small deformation condition is defined as:

$$U = \frac{1}{2} \boldsymbol{\sigma} : \boldsymbol{\epsilon}, \quad (18)$$

where $\boldsymbol{\sigma}$ is the Cauchy stress tensor and $\boldsymbol{\epsilon}$ is engineering strain tensor. This expression can be expanded as:

$$U = \frac{\nu\mu}{1-2\nu} (\varepsilon_{xx} + \varepsilon_{yy} + \varepsilon_{zz})^2 + \mu(\varepsilon_{xx}^2 + \varepsilon_{yy}^2 + \varepsilon_{zz}^2) + \mu(\varepsilon_{xy}^2 + \varepsilon_{yz}^2 + \varepsilon_{zx}^2), \quad (19)$$

Here, ν, μ are the Poisson's ratio and shear modulus respectively. For the isotropic deformation ($\varepsilon_{xx} = \varepsilon_{yy} = \varepsilon_{zz} = \varepsilon$, $\varepsilon_{xy} = \varepsilon_{yz} = \varepsilon_{zx} = 0$) condition, the elastic energy density is ($\nu = 0.25$):

$$U = 3E\varepsilon^2, \quad (20)$$

where E is the elastic modulus. For the case of uniaxial deformation ($\varepsilon_{xx} = \varepsilon$, $\varepsilon_{yy} = \varepsilon_{zz} = \varepsilon_{xy} = \varepsilon_{yz} = \varepsilon_{zx} = 0$), the elastic energy density can be calculated as:

$$U = \frac{3}{5}E\varepsilon^2. \quad (21)$$

The analytical integration of Eq. (5) under the assumptions of spherical horizon and isotropic deformation is derived to build up the relation between c and E . [14, 15]

$$c = \frac{18k}{\pi\delta^4}. \quad (22)$$

However, this relation decays nearby boundary and under non-uniform discretization. In this work, the elastic energy density of a point is enforced to equal the collective energy density of all its bonds under isotropic deformation condition which results in ($\varepsilon = s$):

$$3E = \sum_{\xi} \frac{1}{2}c_X|\xi|\Delta V_{X'}. \quad (23)$$

Eq. (23) indicates that the microelastic modulus c_X is a distributive quantity in contrast with a constant parameter throughout computational domain in the other peridynamics model. c_X depends on the discretization (coarse or fine, uniform or nonuniform) as well as the location of \mathbf{X} . The points nearby boundary have bigger c_X than that located inside domain because the boundary \mathbf{X} has fewer bonds. Theoretically, Eq. (23) requires a linear equation solver to find the solution of c_X . In practice, the analytical solution Eq. (22) can be considered as the initial solution and a couple of iterations in the implicit solving will lead to an accurate estimation of solution for c_X . Due to Eq. (3), it's worthwhile to mention that the bond force with this distributive elastic modulus becomes

$$f(\boldsymbol{\eta}, \boldsymbol{\xi}) = \frac{c_X + c_{X'}}{2} s \frac{\boldsymbol{\xi}}{|\boldsymbol{\xi}|}. \quad (24)$$

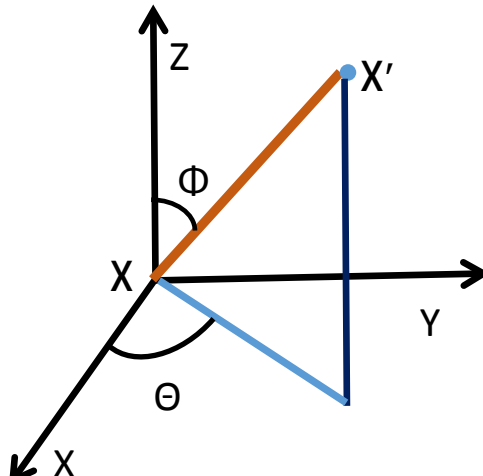


Fig. 2 the sphere coordinates of a bond

Eq. (23) ensures the equivalent elastic energy density under isotropic deformation. The equivalence for other deformation status is not granted. For that reason, an ellipsoid calibration algorithm [14] is utilized to adjust the elastic modulus of a particle to fit the complex stress status. The horizon of a point \mathbf{X} is a sphere with radius δ . Assume a surrounding point \mathbf{X}' has the spherical coordinates (r, ϕ, θ) , shown as Fig. 2. In a specific mesh, an artificial uniaxial deformation along X- axis is defined: $x_1(t) = X_1 + aX_1$, $x_2(t) = X_2$, $x_3(t) = X_3$, here x_i denotes the coordinate at current configuration, a is the deformation along X- axis, we choose $a = 0.001$. In this case, the ratio of real elastic energy (Eq. (21)) and the collective bond energy density (Eq. (6)) can be calculated:

$$T_1 = \frac{\frac{3}{5}Ea^2}{\sum_{\xi} \frac{1}{4}(c_X + c_{X'})|\xi|\Delta V_{X'}}. \quad (25)$$

With the same process, the ratio of real elastic energy (Eq. (21)) and the collective bond energy density along Y- and Z- axis can be evaluated as T_2 , T_3 respectively. T_i is an orientation dependent vector while the microelastic modulus is a scalar. Here an ellipsoid algorithm is adopted to construct a scalar factor to calibrate the microelastic modulus with respect to uniaxial deformations [14]:

$$c_c = \sqrt{\left(\frac{1}{(\cos(\theta) \sin(\phi))^2} + \frac{1}{(\sin(\theta) \sin(\phi))^2} + \frac{1}{(\cos(\phi))^2}\right)}. \quad (26)$$

Eventually, the microelastic modulus was corrected as:

$$c_X = c_c c_X^0, \quad (27)$$

where c_x^0 is the value estimated by Eq. (23). Note that the numerical equivalence procedure described in this section only needs to be performed once in the initialization phase and not needed during the time-marching stage.

5. LS-DYNA® Keywords

In this section, two new keywords are introduced in LS-DYNA® and are used to describe the peridynamics element formula and PMB material respectively.

1) SECTION_SOLID_PERI

Since the discretization formula, Eq. (17), follows the standard finite element derivation, the FEM peridynamics formula is considered as a type of solid element. The element formulation number of the bond-based peridynamics model is set as ELFORM=48. As other solid elements, the 4 nodes, 6 nodes and 8 nodes elements are supported by this new element formulation. The element connectivity data follows the common format defined in LS-DYNA® keywords.

This section keyword has two cards:

Card 1:

Variable	SECID	ELFORM
TYPE	I	I
Default		48

The variables in Card 1 are:

SECID: The user defined section ID.

ELFORM: The element formulation number, set to be 48.

Card 2:

Variable	DR	PTYPE
Type	F	I
Default	1.00	1

The variables in Card 2 are:

DR: $0.8 \leq DR \leq 1.5$ is recommend to determine the horizon size based on the characteristic length of element.

PTYPE: EQ.1: bond-based formula (currently implemented)

EQ.2: state-based formula (reserved for future implementation)

2) MAT_ELASTIC_PERI

The PMB material is an elastic solid material with failure. This material keyword has 1 card.

Card 1

Variable	MID	RO	E	G
Type	I	I	F	F
Default				1.0E28

The variables in Card 1 are:

MID: User defined material ID

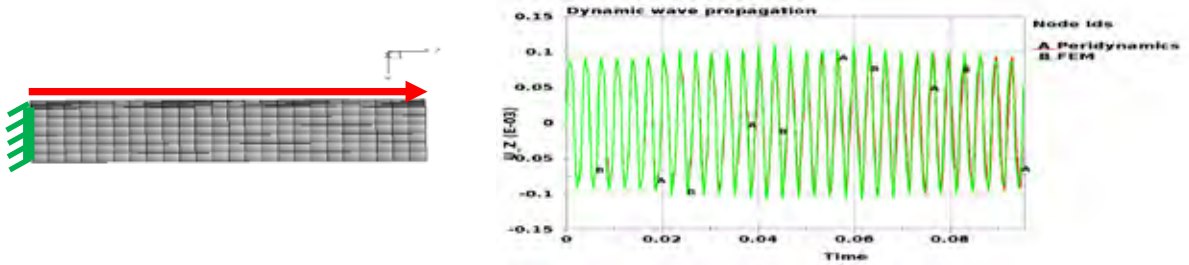
RO: mass density

E: Classic elastic modulus E.

G: Fracture energy release rate G

6. Numerical examples

In this section, five benchmark examples are presented to study the performance of the discontinuous Galerkin bond-based peridynamics formulas and numerical algorithm. The numerical time integration of the discrete equation (Eq. (17)) is performed by the central difference integration algorithm as that in the standard explicit dynamic FEM method. The standard bilinear shape function of 8 nodes elements is used for all examples.



6.1 The wave propagation in 3D bar

Fig. 3 The wave propagation in 3D bar. (a) specimen; (b) the displacement history of the middle point

In dynamic simulations, the stress wave plays a crucial role which induces all the material responses. The peridynamics applications run without stress status. However, the displacement of a particle is an alternative way representing the waves inside solid. A 3D elastic bar ($1.0m \times 1.0m \times 4.0m$) is subjected the initial velocity $V_z = 0.2 m/s$ in the whole specimen and fixed one end, shown as Fig. 3 (a). The material constants are $\rho = 8.0E3kg/m^3$, $E = 190Gpa$. The specimen is discretized by 864 brick elements (8 nodes elements). This problem is carried out by the proposed method as well as the classic FEM method with the same elastic constants and $\nu = 0.25$. Induced by the initial velocity, the elastic specimen oscillates with time along the dynamic wave. The results from bond-based peridynamics model and classic FEM are compared in Fig 3 (b) with the

displacement component u_z of the particle located at middle of the domain. Fig. 3 shows the almost identical curves from peridynamics and FEM which implies the proposed model can capture the dynamic response of material as good as FEM without considering the material failure.

6.2 The consistency of displacement fields in the discontinuous mesh

The discontinuous mesh utilized in this paper doesn't share nodes along the interfaces of adjacent elements. This unique feature ensures the capability of the proposed method to capture the potential discontinuity in the displacement field. These duplicate nodes occupy the same spatial position at the reference configuration, and are supposed to have consistent deformation at current configuration without failure. This numerical example uses the same mesh as in the first example. A prescribed velocity boundary along z direction is applied at one end of the specimen with a linear function of time reaching its maximum of 1.0 m/s at 0.005 s and the opposite end is fixed as shown in Fig. 4. The material constants are the same as used in the first example. With this boundary condition, the specimen will experience a quadratic type of displacement history with the exception of the points located at the fixed end. The displacement histories of particles in the middle of specimen (the middle red line in Fig. 4, marked as A) are illustrated in Fig. 5. (a). In contrast, the particles at the edge of specimen (the red line in Fig. 4, marked as B) are shown in Fig. 5 (b). Because the total number of particles in these lines is large, Fig. 5 neglects the line legends. The top lines in Fig. 5 represent particles at top where the prescribed boundary is imposed on and the bottom line which is a flat line representing the fixed condition. The results show the consistent displacement fields with the analytical curves (the top curves in Fig. 5 (a) and (b)).

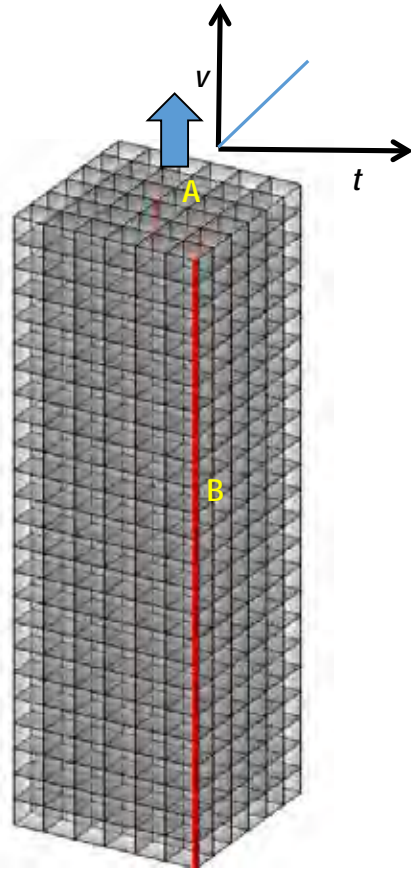
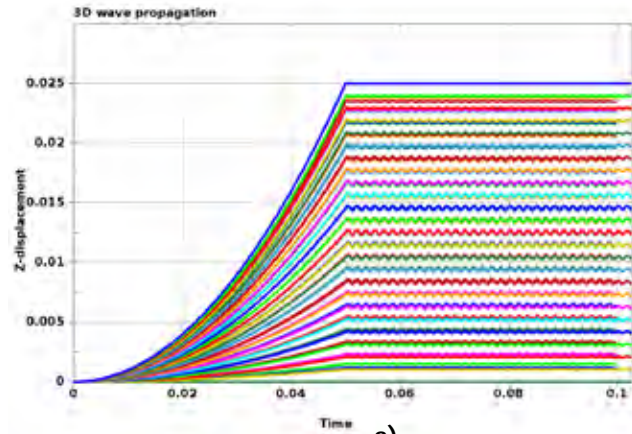
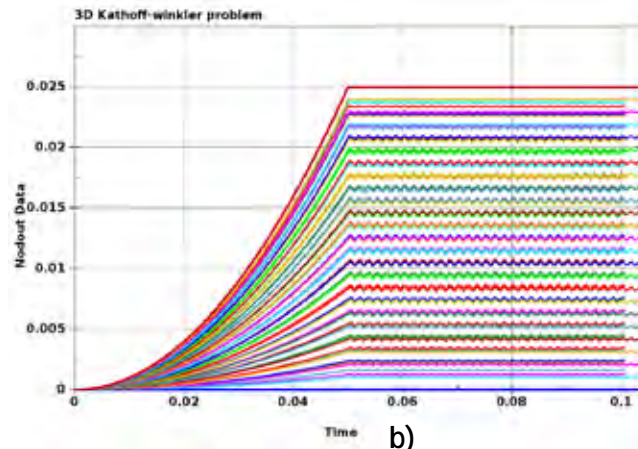


Fig. 4 the specimen configuration



a)



b)

Fig. 5 The displacement history, (a) nodes at the middle, (b) nodes at the edge.

6.3 The convergence of mode-I fracture

In this numerical examples, a rectangular sample ($0.1\text{ m} \times 0.2\text{ m} \times 0.03\text{ m}$) with two pre-cracks are stretched (velocity : 1.0 m/s) at two ends with opposite directions as shown in Fig. 6. Consequently a mode-I crack will initiate and propagate along the initial cracks. The material constants used in this example are: $\rho = 8.0E3\text{ kg/m}^3$ $E = 190\text{ Gpa}$ $G = 5.5E4\text{ J/m}^2$. Three model refinements with 600, 4800, and 38400 elements are utilized to study the convergence of the proposed equations respectively.

The crack lengths of three refinements are compared in Fig. 7. Note the crack length is measured as an approximate value according the time sequence in the damage fringe plots shown in Fig. 8. In Fig. 7, the lengths of initial cracks are the same with different refinements. Stable crack propagation is observed in three mesh models and the curves converge to the finest mesh model. It is interesting to note that the time-crack length curves of three refinements are parallel which imply the same crack propagation speed in different mesh sizes.

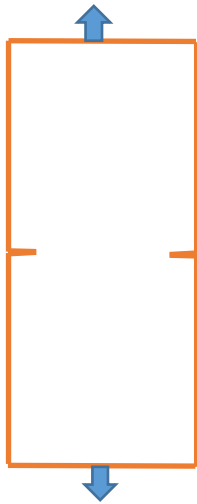


Fig 6 The specimen with preset notches

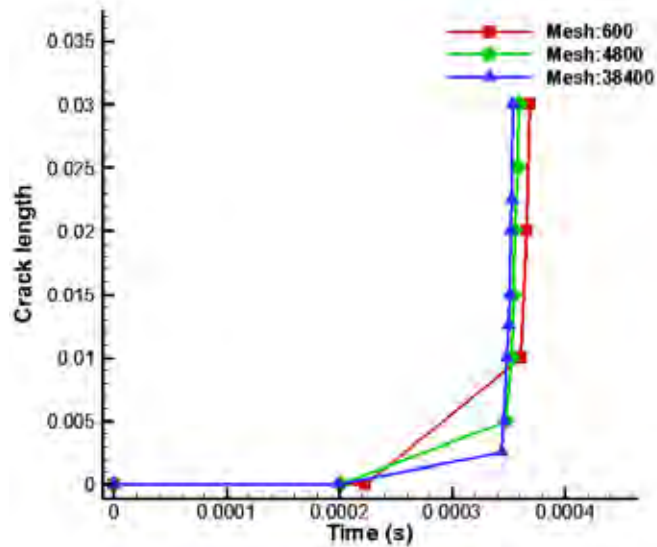


Fig. 7 The convergence of mode I fracture

The damage morphologies of three refinements at $t = 420 \mu s$ are shown in Fig. 8. Here the fringe color represents the value of damage indicator according to Eq. 10. From Fig.8, one can observe that the damage is localized along the crack surface which resembles the mode-I failure in brittle material.

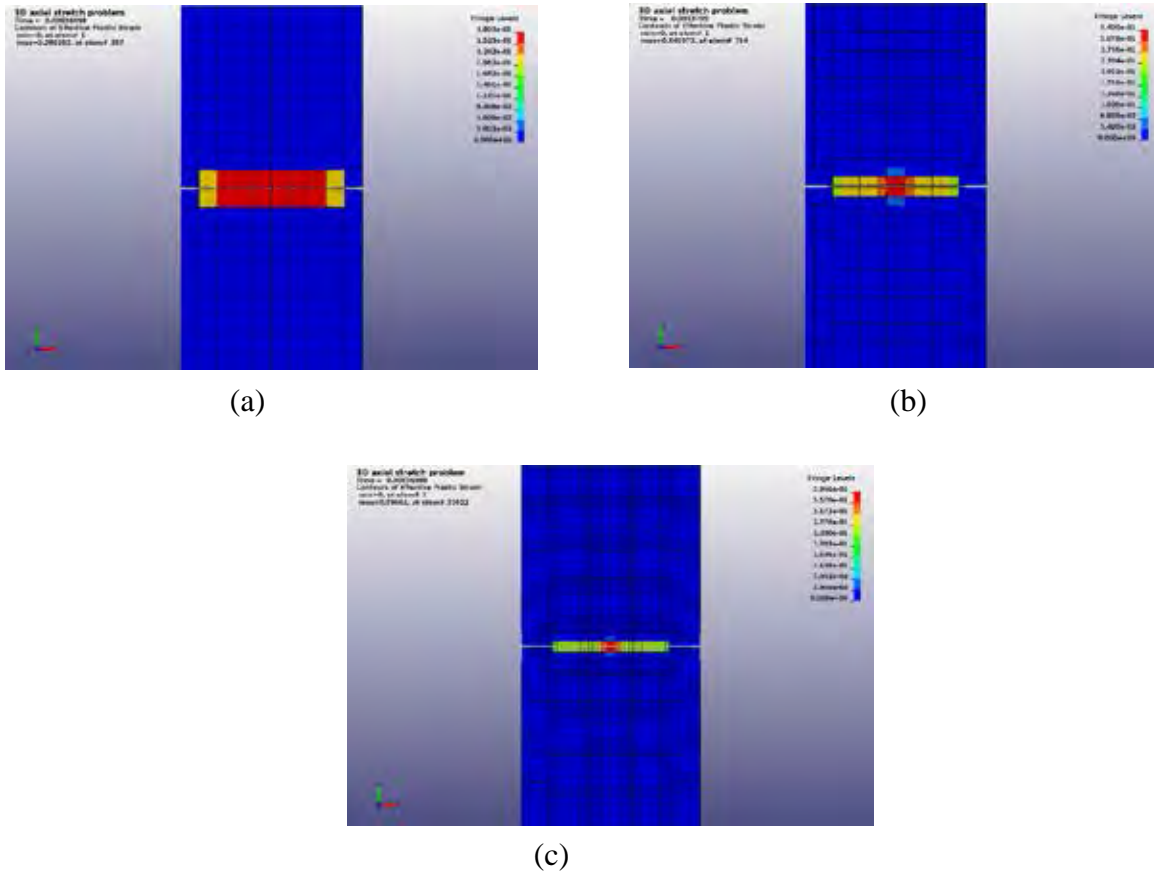


Fig. 8 The damage morphologies of mode I fracture, (a) coarse mesh (600 elements), (b) medium mesh (4800 elements), (c) fine mesh (38400 elements)

6.4 The Kalthoff-Winkler problem

While the numerical advantages of boundary condition and contact/constraint enforcements, spatial integration of non-uniform mesh, coupling with other Galerkin-based numerical methods are embedded in the present method, there is a shortcoming introduced by the mesh-based integration: the crack path only goes along the edges of elements which result in some degrees of mesh dependence of crack path when the mesh is overly coarse. In this example, the Kalthof-Winkler problem [14] which has two tilted cracks is carried out to study the sensitivity of crack propagation path in different mesh size.

The Kalthoff-Winkler experiment concerns the impact of a steel plate with two notches with a cylindrical impactor, Fig. 9. The diameter of the cylindrical impactor is 0.05 m with the mass of 1.57 kg . This simulation considers the impactor as rigid body. To reduce the computational cost, the impactor is represented by a rectangle shell structure with the same mass and interacts with the steel plate through contact. The material constants of the specimen are listed: $\rho = 8.0E3\text{ kg/m}^3$ $E = 190\text{ Gpa}$ $G = 6.0E4\text{ J/m}^2$. To study the convergence of the solution, the specimen is discretized with three refinements: the coarse mesh with 30800 elements, the medium mesh with 52272 elements and fine mesh with 97608 elements.

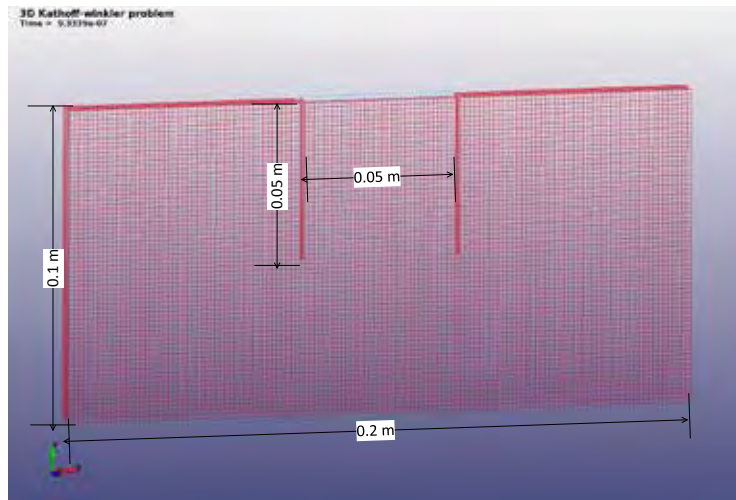


Fig .9 The dimension of specimen in Kalthoff-Winkler problem

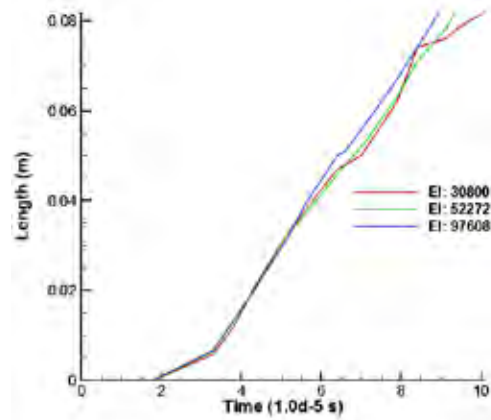
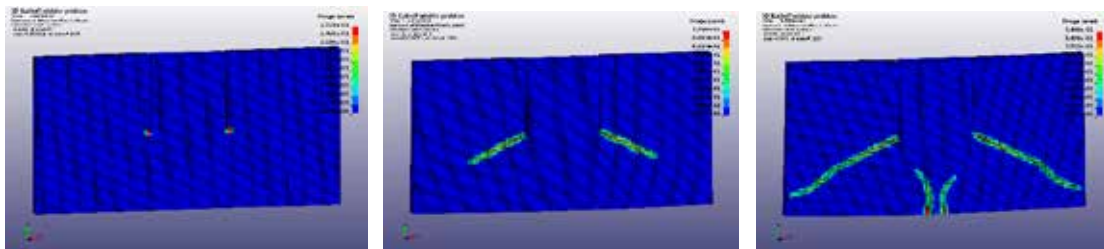


Fig. 10 The crack length history of Kalthoff-Winkler problem

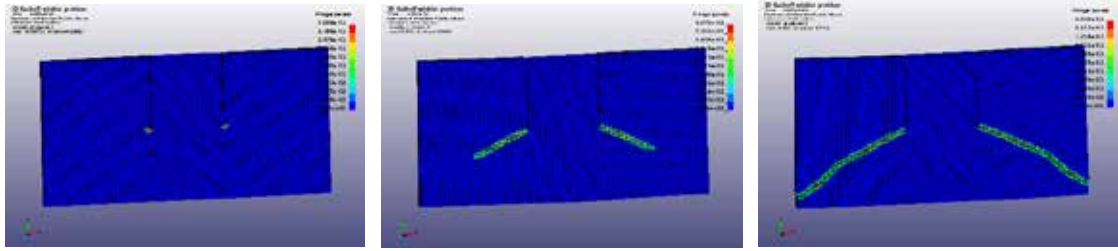
The history of crack length in three mesh models is shown in Fig. 10 which indicates a convergence of the solution. The time sequence of the failure process with different meshes is illustrated in Fig. 11 with the contour of damage indicator. While the main crack path in three mesh models has the angle about 68° as seen in the experimental results, the result of coarse mesh with 30800 elements predicts the secondary cracks. The secondary cracks do not shown up in the result of two refined mesh models. This result suggests that the discretization of the FEM peridynamics model should be relatively refined in order to prevent the mesh size sensitivity and achieved the desired accuracy. However, the convergent solution is expected when the discretization model is continuously refined.



(a) $t = 29 \mu s$

(b) $t = 59 \mu s$

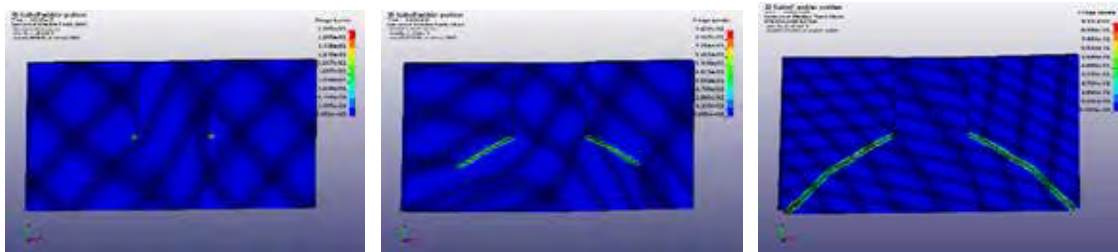
(c) $t = 110 \mu s$



(d) $t = 29 \mu s$

(e) $t = 59 \mu s$

(f) $t = 110 \mu s$



(g) $t = 29 \mu s$

(h) $t = 59 \mu s$

(i) $t = 110 \mu s$

Fig. 11 The time sequence of damage process, background: damage indicator, (a)-(c): the coarse mesh; (d)-(f): medium mesh; (g)-(i):fine mesh

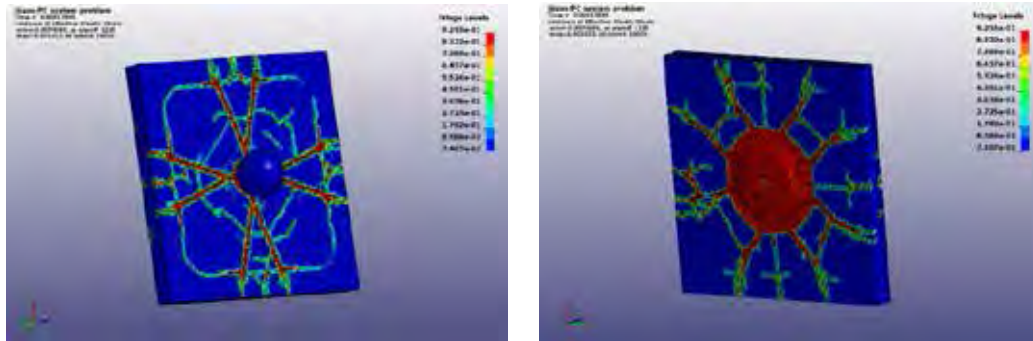
6.5 Impact damage on the glass-polycarbonate-glass structure

One of the major applications of bond-based peridynamics which concerns the brittle material is the damage prediction of windshield in the automotive industry. In contrast with the house windows, auto windshield is made of a three layer structure of glass-polycarbonate (pc)-glass as shown in Fig. 12. Hu et al. [25] reported their research on the experimental and numerical damage prediction of glass-PC structure using the standard bond-based peridynamics. Bobaru et al. [26] presented the numerical prediction of glasses-pc system where 7 glass layers stack on one PC layer. This numerical example follows most of their experimental settings and the material constants except another glass layer is attached on the bottom of the PC layer, i.e., the specimen becomes a glass-PC-glass structure as that shown in Fig. 13. In the experiment, the glass layers are clamped by a metal frame with a square hole of $5.08 \text{ cm} \times 5.08 \text{ cm}$. As shown in the study by Hu et al.

[25] and Bobaru et al. [26], this clamp contact boundary condition is simplified as the fixed out-of-plane boundary condition in the contact zone (Fig 13, the red ring at the top and bottom surface). The glass is soda-lime glass with material properties given by: $\rho = 2.44E3 \text{ kg/m}^3$, $E = 72Gpa$, $G = 8.0 \text{ J/m}^2$ [25]. The projectile is treated as a rigid body with material constants given by $\rho = 3.73E3 \frac{\text{kg}}{\text{m}^3}$, $E = 210Gpa$, $\nu = 0.3$. This density leads to a total mass of 0.692 g for projector. The projector is placed nearby the middle of the top surface with the initial velocity: $V_z = -31.0 \text{ m/s}$. Because no damage is observed in the PC layer from experiments [25], the PC layer is considered a simple elastic material with $\rho = 1.2E3 \frac{\text{kg}}{\text{m}^3}$, $E = 2.0Gpa$, $\nu = 0.25$. There is no adhesive between glasses and PC layers in the experiments. Therefore, no cohesive elements are placed in the glass-PC and PC-glass interfaces for this numerical study. Instead, contacts are assumed in these interfaces and the projector-glass interface (the red surfaces in the middle of Fig. 13). The glass-PC-glass specimen is discretized by 100,000 elements for glasses, 2500 elements for PC layer and the projector is simulated by one layer of brick elements at surface with 1014 elements shown in Fig. 13.

The damage patterns of the specimen are shown in Fig 14. Most damage patterns observed in the experiment are reproduced in this numerical simulation: the ripple cracks in the ellipses, the splitting cracks in the circles, through-thickness tilted cracks in the diamonds and boundary cracks in triangles. On the top surface of the glass, the main failure pattern consists of diagonal cracks and circle cracks nearby the impact zone. At the bottom surface, there is a main damage circle zone and the diagonal cracks extend from this zone as shown Figs. 15 (a) and (b). This damage pattern is well recognized in the failure analysis of windshield applications. The section damage pattern of the glass-PC-glass system is shown in Fig. 16 where a clear cone shape damage zone which is found in other glass indentation experiments [27] is observed using the proposed method. The contact reaction force reacting on the projector is presented in Fig 17. The dynamic damage process is

Fig. 14 Damage pattern in the glass



(a)

(b)

Fig. 15 The damage status by impaction, (a) the top surface; (b) the bottom surface

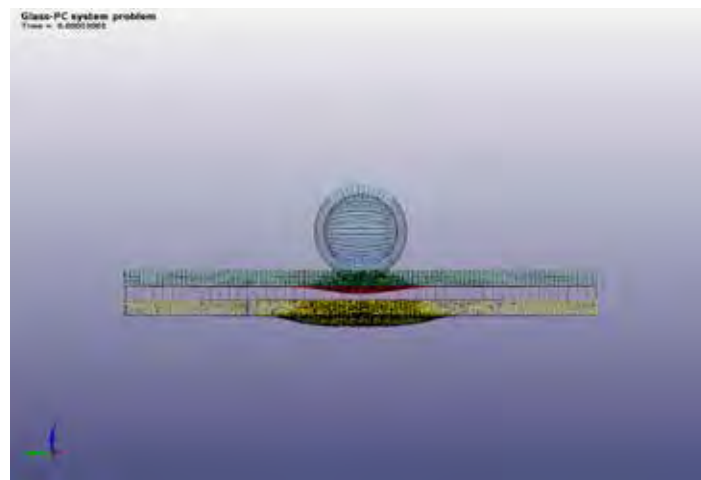


Fig. 16 The cone shape in global damage zone

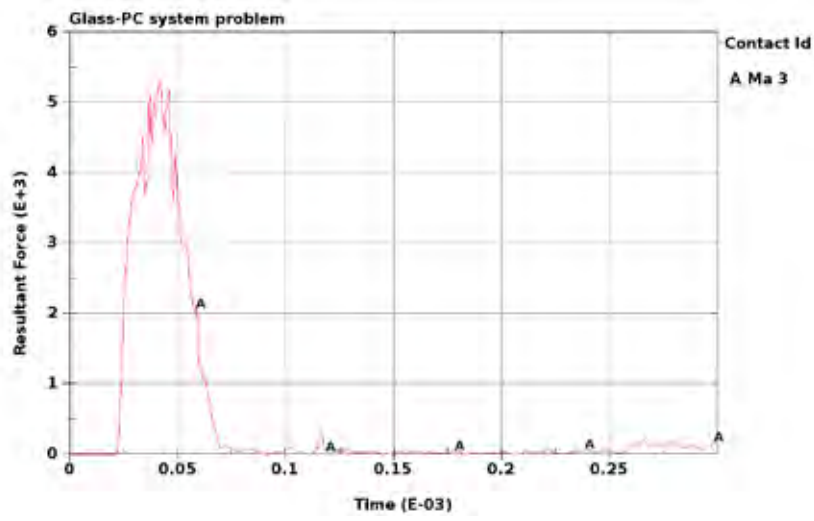
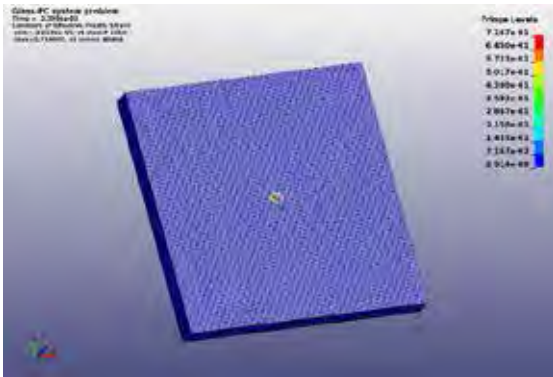
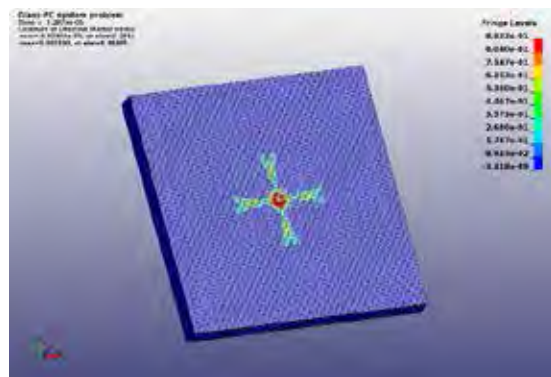


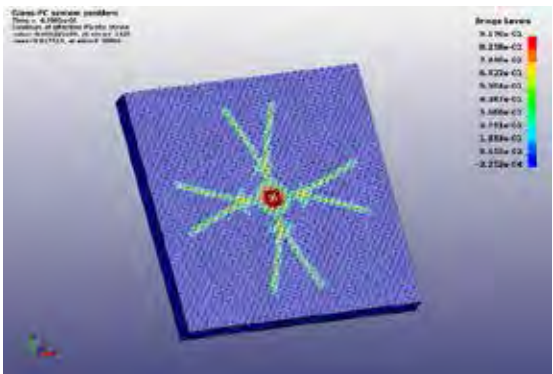
Fig. 17 The contact force history on the ball



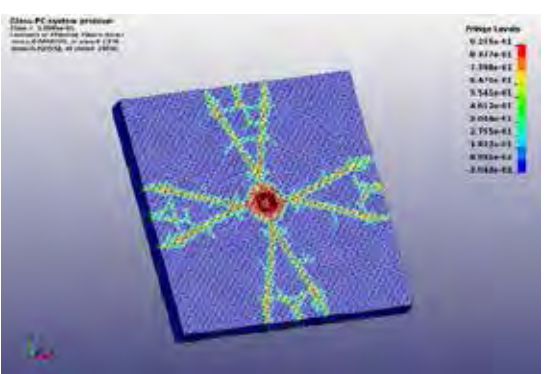
(a) $t = 24 \mu\text{s}$



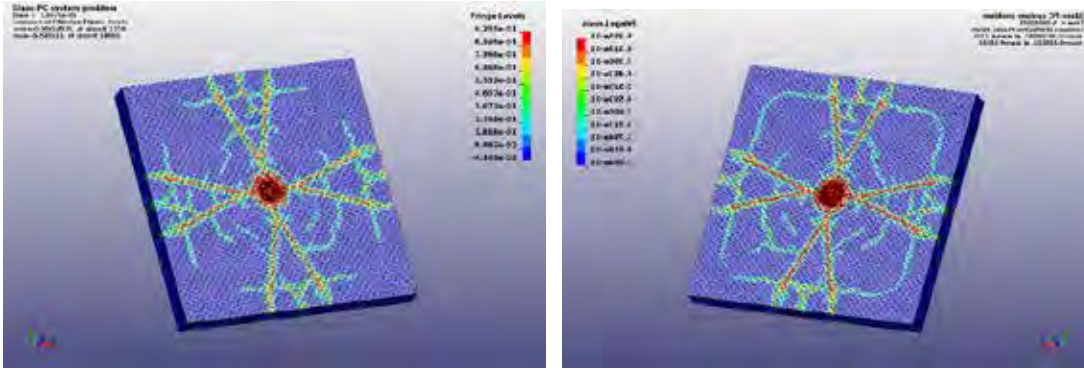
(b) $t = 33 \mu\text{s}$



(c) $t = 44 \mu\text{s}$



(d) $t = 69 \mu\text{s}$



(e) $t = 79 \mu s$

(f) $t = 100 \mu s$

Fig. 18 The time sequence of damage process, background: damage indicator

7. Conclusion

This paper presents the formulas and numerical algorithms to predict the damage of brittle material by the bond-based peridynamics model. In contrast to the meshfree peridynamics, the Galerkin weak form of the peridynamics governing equations is constructed with the two-levels of spatial integrations: the computational domain integration and horizon integration. In order to represent the moving strong discontinuities in the dynamics damage process, the solution is approximated as the element-wise discontinuous field by the regular FEM shape function. There are several practical advantages to implement the bond-based peridynamics model in the FEM framework due to the intrinsic features of FEM method. First, the boundary condition enforcement is straightforward because the FEM shape functions satisfy the Kronecker-delta property. Second, the Gaussian integration can reduce the mesh dependence in the case of non-uniform mesh. Third, the mesh-based calculation represents the material boundary explicitly. Consequently, the existing contact algorithms can be utilized by the peridynamics parts to couple with other regular FEM parts.

As a nonlocal model, the numerical treatment varies with non-uniform discretization and nearby boundary when a uniform micro elastic modulus is assigned to all peridynamics

points. This numerical procedure was implemented in LS-DYNA[®] which calculates the specific micro elastic modulus for each particle based on its horizon to assure an equivalent elastic energy density with the classic mechanics theory. Therefore the non-failure material constant of the PMB material in the LS-DYNA[®] keyword only requires the classic elastic modulus E instead of the micro elastic modulus c . Though the failure in bond-based peridynamics is a nonlocal status, the LS-DYNA[®] keyword uses the classic energy release rate as failure criteria which determine the critical bond stretch basing on the equivalent energy to form a crack surface.

Several numerical examples are carried out to study the performance of the proposed method. The results illustrate that the method can capture the dynamic response of elastic solid as the classic FEM method before damage happens. In the damage process, the method can predict the dynamic process of mixed modes fracture, multi-cracks fracture and fragmentation effectively and accurately. An application of the method to the anisotropic elastic material is under implementation and will be presented in the near future.

Acknowledgment

The authors wish to thank Dr. John O. Hallquist of LSTC for his support to this research. Helpful discussions with Dr. Stewart Silling and Dr. David John Littlewood of Sandia National Laboratories, Dr. Gilles Lubineau and Dr. Fei Han from King Abdullah University of Science and Technology, and Dr. Hamid Razi from Boeing Company are gratefully acknowledged.

References

- [1] Moës N., Dolbow J., Belytschko T. A finite element method for crack growth without remeshing. *International Journal for Numerical Methods in Engineering* 1999; 46: 133–150.
- [2] Xu X.P., Needleman A. Numerical simulations of fast crack growth in brittle solids. *Journal of the Mechanics and Physics of Solid*. 1994; 42:1397–1434.

- [3] Ren B., Li, S.F. Modeling and simulation of large-scale ductile fracture in plates and shells. *International Journal of Solids and Structures* 2012, 49: 2373–2393.
- [4] Kroner E. Elasticity theory of materials with long range forces. *Int. J. Solids Struct.* 1967; 3:731-742.
- [5] Chen J.S., Wu C.T., Belytschko T. Regularization of material instabilities by meshfree approximations with intrinsic length scales. *Int. J. Numer. Methods Eng.* 2000; 47:1303-1322.
- [6] Silling S.A. Reformulation of elasticity theory for discontinuities and long-range forces. *Journal of the Mechanics and Physics of Solids* 2000; 48:175–209.
- [7] Silling, S.A., Epton, M., Weckner, O., Xu, J., Askari, E., Peridynamics states and constitutive modeling. *J. Elast.* 2007; 88:151-184.
- [8] Bobaru F, Hu W. The meaning, selection, and use of the peridynamics horizon and its relation to crack branching in brittle materials. *International Journal of Fracture* 2012; 176:215–222.
- [9] Gerstle W, Sau N, Silling SA. Peridynamic modeling of concrete structures. *Nuclear Engineering and Design* 2007; 237:1250–1258.
- [10] Askari E, Xu J, Silling S. Peridynamic analysis of damage and failure in composites. *44th AIAA Aerospace Sciences Meeting and Exhibit*, Reno, Nevada, 2006; 1–12.
- [11] Kilic B, Madenci E, Ambur D.R. Analysis of brazed single-lap joints using the peridynamics theory. *47th AIAA/ASME/ASCE/AHS/ASC Structures, Structural Dynamics, and Materials Conference*, Newport, Rhode Island, 2006; 1.
- [12] Lai X, Ren B., Fan H.F., Li, S.F., Wu C.T., Rugeiro R.A and Liu L.S. Peridynamics simulations of geomaterial fragmentation by impulse loads. *Int. J. Numer. Anal. Meth. Geomech.* 2015; 39:1304–1330.

- [13] Warren TL, Silling S.A., Askari A, Weckner O, Epton MA, Xu J. A non-ordinary state-based peridynamic method to model solid material deformation and fracture. *International Journal of Solids and Structures* 2009; 46:1186–1195.
- [14] Madenci E., Oterkus E. *Peridynamic Theory and Its Applications*. Springer, New York, 2014.
- [15] Wu, C. T. Kinematic constraints in the state-based peridynamics with mixed local/nonlocal gradient approximations. *Computational Mechanics* 2014; 54: 1255-1267.
- [16] Wu, C. T., Ren, B. A stabilized non-ordinary state-based peridynamics for the nonlocal ductile material failure analysis in metal machining process. *Computer Methods in Applied Mechanics and Engineering*, 2015; 291:197-215.
- [17] Silling S.A., Askari E. A meshfree method based on the peridynamic model of solid mechanics. *Computers and Structures* 2005, 83:1526–1535.
- [18] Macek R.W., Silling, S.A. Peridynamics via finite element analysis. *Finite Elements in Analysis and Design* 2007, 43:1169-1178.
- [19] Chen X., Gunzburger M. Continuous and discontinuous finite element methods for a peridynamics model of mechanics. *Comput. Methods Appl. Mech. Engrg.* 2011, 200:1237-1250.
- [20] Du Q., Zhou K. Mathematical Analysis for the Peridynamic Nonlocal Continuum Theory. *ESAIM: Mathematical Modelling and Numerical Analysis* 2011, 45: 217-234.
- [21] Zhou K., Du Q. Mathematical and Numerical Analysis of Linear Peridynamic Models with Nonlocal Boundary conditions. *SIAM J. NUMER. ANAL.* 2010, 48(5):1759-1780.

- [22] Lubineau G., Azdoud Y., Han F., Rey C., Askari A. A morphing strategy to couple non-local to local continuum mechanics. *Journal of the Mechanics and Physics of Solids* 2012, 60:1088-1102.
- [23] Azdoud Y., Han F., Lubineau G. The morphing method as a flexible tool for adaptive local/non-local simulation of static fracture. *Comput. Mech.* 2014, 54:711-722.
- [24] Shu C.W. Discontinuous Galerkin Method for Time-Dependent Problems: Survey and Recent Developments Chapter in Recent Developments in Discontinuous Galerkin Finite Element Methods for Partial Differential Equations. Springer, New York, 2013.
- [25] Hu W., Wang Y., Yu J., Yen C.F., Bobaru F. Impact damage on a thin glass plate with a thin polycarbonate backing. *International Journal of Impact Engineering* 2013, 62:152-165.
- [26] Bobaru, F., Ha Y.D., Hu W. Damage progression from impact in layered glass modeled with peridynamics. *Central European Journal of Engineering* 2012, 2(4):551-561.
- [27] Benbow J. Cone Cracks in Fused Silica. *Proceedings of the Physical Society*, 1959 75(5): 697-699.

Best Fit and Its Application in Metal Forming

Xinhai Zhu, Li Zhang, Yuzhong Xiao
LSTC

INTRODUCTION

In springback prediction and compensation process simulation, there is always a need to assess the accuracy of the springback prediction using physical white-light scanned parts. This keyword rigidly moves two parts so that they maximally coincide. It can be used in sheet metal forming to translate and rotate a springback part (source) to a scanned part (target) to assess springback prediction accuracy. This keyword is applicable to shell elements only.

MAIN FEATURES/EXAMPLES

Scanned parts are typically given in the *STL* format, which can be imported into *LS-PrePost* and written back out as a keyword mesh file. The converted scanned keyword file can be used as **FILENAME** as a target mesh in an input file (see Example 1). The predicted springback mesh (with **NODE*, **ELEMENT_SHELL*, **CONSTRAIN_ADAPTIVITY* cards only) can be included in the input file using **INCLUDE*. The best-fit program uses an iterative least-squares method to minimize the separation distances between the two parts, eventually transforming the springback mesh (source) into the position of the target mesh (scan). The normal distances between the two parts are calculated after the best-fitting, and stored as thickness values in a file **bestfit.out**, which is essentially a *dynain* file.

Both positive and negative distances are calculated and stored as the *Thickness*. Color contours of the normal distances between the two parts can then be plotted using *COMP→Thickness*. Positive distance means the source mesh is above the target mesh in a larger coordinates, and negative distance is below the target mesh in a smaller coordinates. For areas where no corresponding meshes can be found between the two parts, the distances are set to nearly zero. The fitting accuracy is within 0.02mm.

The scan file (*STL*) mesh can be coarsened in a scan-processing software from a typically very dense mesh to a more reasonably sized mesh to reduce the computing time. In any case, the coarser mesh should be selected as the target mesh for optimal computational speed.

The fitted mesh and target mesh parts can both be imported into *LS-PrePost*. Using the *SPLANE* feature in *LS-PrePost*, multiple sections can be cut on both parts to assess springback deviations on a cut-section basis.

It is suggested that the orientation of the included file (source) should be within 30 degrees in any direction of the target file. In addition, the more rotations needed to re-orient the include file to align with the target file, the more CPU time will it take to complete the best fitting.

In case the source mesh orients more than 30 degrees in any directions of the target mesh, NSETS and NSETT can be used to initially align the source mesh to the target mesh before a full best-fit is performed. See **Example 3** and Figure 1.

To improve computing speed, the variable NSKIP can be used during bucket sorting. Two options are available. The positive option is to specify the number of nodes to skip during bucket searching; the negative option is to specify a distance. Usually a distance of 5 mm is sufficient to achieve a good fit. In the Table below, computing speed and the max/min deviations from the springback mesh to the target scan for an automotive part are shown, under various combinations of NSKIP and IFAST. All runs were made on a 1 CPU XEON E5520 machine, with 685132 elements on the target scan and 135635 elements on the springback mesh.

NSKIP	IFAST=0		IFAST=1	
	CPU time	Max/Min (mm)	CPU time	Max/Min (mm)
2	10 min 38 sec	1.28/-1.59	4 min 3 sec	1.22/-1.59
5	4 min 49 sec	1.21/-1.59	1 min 59 sec	1.25/-1.61
10	2 min 46 sec	1.27/-1.59	1 min 18 sec	1.44/-1.53
20	1 min 24 sec	1.27/-1.59	59 sec	1.42/-1.64
50	50 sec	1.22/-1.61	40 sec	1.43/-1.67

Example 1 – fitting with all nodes from the included file:

A complete input example is provided below to best fit a mesh part spbk_NoSS.k with PID 4 to the target mesh part scan.k with PID 1. NSKIP is set to “2” and speed optimization is activated by setting IFAST to “1”. Both parts can be modeled as rigid bodies.

```
*KEYWORD
*PARAMETER_EXPRESSION
I pidscan 1
I pidspbk 4
*CONTROL_FORMING_BESTFIT
$ IFIT NSKIP GAPONLY IFAST IFSET
  1 2 0 1 0

scan.k
*INCLUDE
spbk_NoSS.k
*PART
scan data
$ PID SID MID
  &pidscan 1 1
springback mesh
$ PID SID MID
  &pidspbk 1 1
*MAT_RIGID
$ MID RO E PR
  1 0.780E-02 1.648E+05 0.280E+00
$ CMO CON1 CON2
  1.0 7.0 7.0

$LCO

$-----
```

```

*SECTION_SHELL
$   SECID   ELFORM   SHRF   NIP
      1       2           1
$   T1      T2      T3      T4
      1.0    1.0    1.0    1.0
$-----
*END

```

Example 2 – fitting with nodes excluded from a node set:

From the last example, the included file `spbk_NoSS.k` now consists of node set 128. The node set, which may feature geometry that are not a part of the scan target, is being excluded (`IFSET=-128`) from participating in the best fitting.

```

*KEYWORD
*PARAMETER_EXPRESSION
I pidscan      1
I pidspbk      4
*CONTROL_FORMING_BESTFIT
$   IFIT   NSKIP   GAPONLY   IFAST   IFSET
      1     2       0         1     -128

scan.k
*INCLUDE
spbk_NoSS.k
*PART
scan data
$   PID     SID     MID
  &pidscan  1       1
springback mesh
$   PID     SID     MID
  &pidspbk  1       1
*MAT_RIGID
$   MID     RO      E      PR
      1 0.780E-02 1.648E+05 0.280E+00
$   CMO     CON1    CON2
      1.0   7.0    7.0
$LCO

$-----
*SECTION_SHELL
$   SECID   ELFORM   SHRF   NIP
      1       2           1
$   T1      T2      T3      T4
      1.0    1.0    1.0    1.0
$-----
*END

```

Example 3 – fitting with NSETS and NSETT:

In the following partial keyword example (shown in Figure 1) a source mesh `sourcemesk.k` is being best fitted to a target mesh `targetmesh.k`. A node set with ID 1 on the source mesh is defined consisting of nodes 1001 1002 and 1003 and a corresponding node set with ID 2 on the target mesh is defined and consists of nodes 1, 2 and 3.

Node ID 1001 and 1 are both located at the center of a dart on the top surface of the hat-shaped part. Node ID 1002 and 2 are selected at the center of an arc of a cutout hole. Lastly, node ID 1003 and 3 are at the center of a tangent line of a radius. With the NSKIP set a “-5”, the search will be done skipping every 5 mm of distance. In this example, since the source and target meshes are exactly the same, the normal distance, as displayed by “*thickness*” is nearly zero everywhere.

```
*CONTROL FORMING_BESTFIT
$---+-----1-----+-----2-----+-----3-----+-----4-----+-----5-----+-----6-----+-----7-----+-----8
$#   IFIT      NSKIP   GAPONLY   IFAST   IFSET     NSETS    NSETT
      1         -5       0         1       0         1         2
$#  FILENAME
targetmesh.k
*INCLUDE
sourcemesk.k
*SET_NODE_LIST
1
1,2,3
*SET_NODE_LIST
2
1001,1002,1003
```

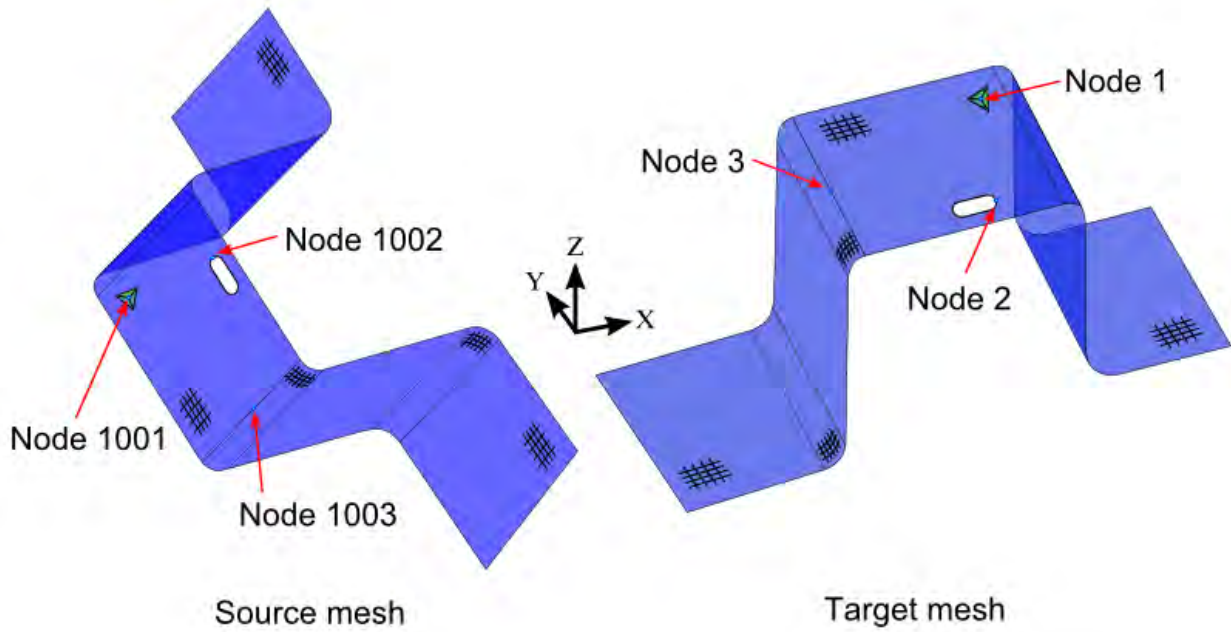
REVISION INFORMATION

This feature is available starting from LS-DYNA Revision 96427 double precision SMP.

- 1) Revision 96696: IFSET is available.
- 2) Revision 99369: NSETS, NSETT are available.

SUMMARY

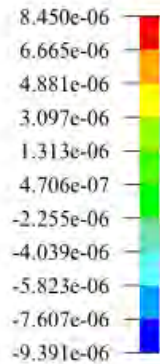
Development of the best-fitting program for metal forming application enables an easy yet powerful way for our users to assess their springback prediction accuracy. It does not require a downloading of a dedicated GUI software. It is simple to use with fast computing speed and it proves to be very robust.



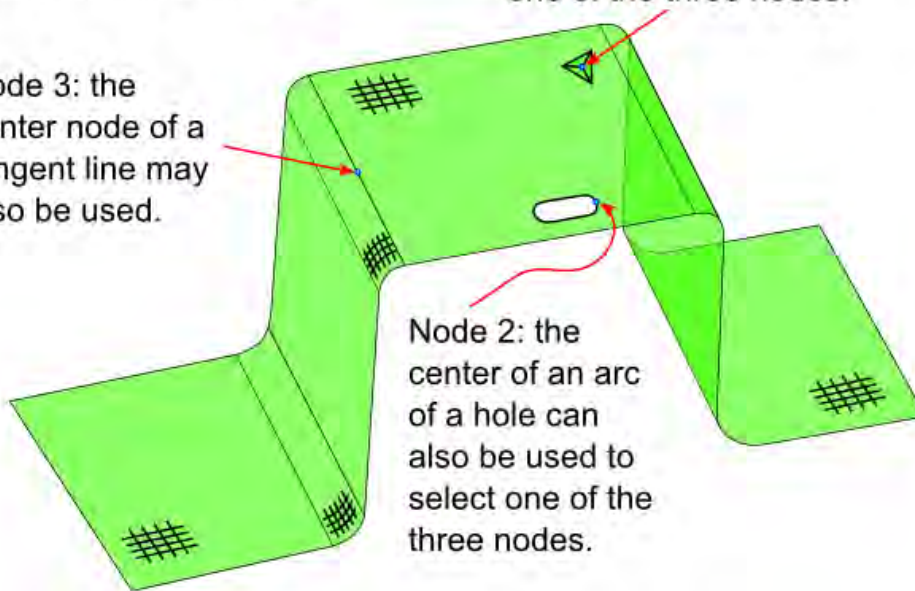
Best fit results of part separation
 Contours of shell thickness
 min=-9.39123e-06 at elem# 102
 max=8.45032e-06 at elem# 149

Node 1: geometry feature
 such as the center of a dart
 is a preferred choice to be
 one of the three nodes.

Part Separation
 (mm)



Node 3: the
 center node of a
 tangent line may
 also be used.



Node 2: the
 center of an arc
 of a hole can
 also be used to
 select one of the
 three nodes.

Best fit results - color contour of part separation plotted with
 "thickness" from the output file "Bestfit.out"

Figure 1. Best fit of two meshes with orientations greater than 30 degrees from each other.